

# Probing SUSY effects in $K_S^0 \rightarrow \mu^+ \mu^-$

Veronika Chobanova,<sup>a</sup> Giancarlo D'Ambrosio,<sup>b</sup> Teppei Kitahara,<sup>c,d</sup>  
 Miriam Lucio Martínez,<sup>a</sup> Diego Martínez Santos,<sup>a</sup> Isabel Suárez Fernández<sup>a</sup>  
 and Kei Yamamoto<sup>e,f</sup>

<sup>a</sup>*Instituto Galego de Física de Altas Enerxías (IGFAE), Universidade de Santiago de Compostela, Rúa de Xoaquín Díaz de Rábago, s/n E-15782 Santiago de Compostela, Spain*

<sup>b</sup>*INFN — Sezione di Napoli, Via Cintia, 80126 Napoli, Italia*

<sup>c</sup>*Institute for Theoretical Particle Physics (TTP), Karlsruhe Institute of Technology, Engesserstraße 7, D-76128 Karlsruhe, Germany*

<sup>d</sup>*Institute for Nuclear Physics (IKP), Karlsruhe Institute of Technology, Hermann-von-Helmholtz-Platz 1, D-76344 Eggenstein-Leopoldshafen, Germany*

<sup>e</sup>*Department of Physics, Nagoya University, Nagoya 464-8602, Japan*

<sup>f</sup>*Kobayashi-Maskawa Institute for the Origin of Particles and the Universe, Nagoya University, Nagoya 464-8602, Japan*

*E-mail:* [Veronika.Chobanova@cern.ch](mailto:Veronika.Chobanova@cern.ch), [gdambros@na.infn.it](mailto:gdambros@na.infn.it),  
[teppey.kitahara@kit.edu](mailto:teppey.kitahara@kit.edu), [miriam.lucio@cern.ch](mailto:miriam.lucio@cern.ch),  
[Diego.Martinez.Santos@cern.ch](mailto:Diego.Martinez.Santos@cern.ch), [isfer@undo-r.com](mailto:isfer@undo-r.com),  
[yamamoto@kmi.nagoya-u.ac.jp](mailto:yamamoto@kmi.nagoya-u.ac.jp)

**ABSTRACT:** We explore supersymmetric contributions to the decay  $K_S^0 \rightarrow \mu^+ \mu^-$ , in light of current experimental data. The Standard Model (SM) predicts  $\mathcal{B}(K_S^0 \rightarrow \mu^+ \mu^-) \approx 5 \times 10^{-12}$ . We find that contributions arising from flavour violating Higgs penguins can enhance the branching fraction up to  $\approx 35 \times 10^{-12}$  within different scenarios of the Minimal Supersymmetric Standard Model (MSSM), as well as suppress it down to  $\approx 0.78 \times 10^{-12}$ . Regions with fine-tuned parameters can bring the branching fraction up to the current experimental upper bound,  $8 \times 10^{-10}$ . The mass degeneracy of the heavy Higgs bosons in MSSM induces correlations between  $\mathcal{B}(K_S^0 \rightarrow \mu^+ \mu^-)$  and  $\mathcal{B}(K_L^0 \rightarrow \mu^+ \mu^-)$ . Predictions for the  $CP$  asymmetry in  $K^0 \rightarrow \mu^+ \mu^-$  decays in the context of MSSM are also given, and can be up to eight times bigger than in the SM.

**KEYWORDS:** Supersymmetry Phenomenology

ARXIV EPRINT: [1711.11030](https://arxiv.org/abs/1711.11030)

---

## Contents

<b>1</b>	<b>Introduction</b>	<b>2</b>
<b>2</b>	<b>Formalism</b>	<b>2</b>
2.1	Definitions	2
2.2	Observables	3
2.3	$K^0 \rightarrow \mu^+ \mu^-$	4
2.4	$\varepsilon'_K / \varepsilon_K$	10
2.5	$\varepsilon_K$ and $\Delta M_K$	12
<b>3</b>	<b>Parameter scan</b>	<b>14</b>
<b>4</b>	<b>Results</b>	<b>15</b>
4.1	Effects from $\left(\delta_d^{LL(RR)}\right)_{12}$ separately	16
4.2	Floating $LL$ and $RR$ MIs simultaneously	17
4.3	Non degenerate Higgs masses	19
<b>5</b>	<b>Conclusions</b>	<b>19</b>
<b>A</b>	<b>Wilson coefficients</b>	<b>21</b>
A.1	$ \Delta S  = 1$ gluino box contribution	21
A.2	$ \Delta S  = 1$ chargino-mediated $Z$ -penguin contribution	25
A.3	$ \Delta S  = 1$ chromomagnetic dipole contribution	25
A.4	$ \Delta S  = 2$ gluino box contribution	25
A.5	Sub-leading contributions to $\varepsilon_K$	26
<b>B</b>	<b>Loop functions</b>	<b>26</b>
B.1	$K^0 \rightarrow \mu^+ \mu^-$	26
B.2	$\varepsilon'_K / \varepsilon_K$	27
B.2.1	$ \Delta S  = 1$ gluino box contributions	27
B.2.2	Chromomagnetic-dipole operator	27
B.3	$\varepsilon_K$	28
B.3.1	$ \Delta S  = 2$ gluino box contributions	28
B.3.2	Wino and Higgsino contributions	28

---

## 1 Introduction

Leptonic decays of pseudoscalar mesons with down-type quarks are known to be very sensitive to the Higgs sector of the Minimal Supersymmetric Standard Model (MSSM), due to, among others, enhancement factors proportional to  $(\tan^6 \beta / M_A^4)$ .<sup>1</sup> This factor comes from the so-called non-holomorphic Yukawa terms at large  $\tan \beta$  [1–6],<sup>2</sup> which are triggered by the supersymmetric (SUSY)  $\mu$  term, and hence the non-SUSY two-Higgs-doublet model cannot produce this enhancement [5]. The best known example is  $B_s^0 \rightarrow \mu^+ \mu^-$  [1–6, 10–18]. If Minimal Flavour Violation (MFV) is imposed, then  $B_s^0 \rightarrow \mu^+ \mu^-$  is the dominant constraint in  $P \rightarrow \mu^+ \mu^-$  decays. This is due to the stronger Yukawa coupling of the  $b$ -quark compared to the  $s$ -quark, and to the better experimental precision in  $B_s^0 \rightarrow \mu^+ \mu^-$  compared to  $B_d^0 \rightarrow \mu^+ \mu^-$ . However, in the presence of new sources of flavour violation, the sensitivity of each mode depends on the flavour and  $CP$  structures of the corresponding terms. Hence, a priori,  $B_s^0 \rightarrow \mu^+ \mu^-$ ,  $B_d^0 \rightarrow \mu^+ \mu^-$ ,  $K_S^0 \rightarrow \mu^+ \mu^-$ , and  $K_L^0 \rightarrow \mu^+ \mu^-$  are all separate constraints that carry complementary information in the general MSSM. The observables related to these decay modes are typically branching fractions and  $CP$  asymmetries. Even though the muon polarization could carry interesting information, it cannot be observed by current experiments.

In this paper, we focus on the MSSM effects in the  $K_S^0 \rightarrow \mu^+ \mu^-$  decay. The Standard Model (SM) expectation is  $(5.18 \pm 1.50_{\text{LD}} \pm 0.02_{\text{SD}}) \times 10^{-12}$  [19–21], where the first uncertainty comes from the long-distance (LD) contribution and the second one comes from the short-distance (SD) contribution. On the other hand, the current experimental upper bound is  $8 \times 10^{-10}$  at 90% C.L., using  $3 \text{ fb}^{-1}$  of LHCb data [22]. The LHCb upgrade could reach sensitivities at the level of about  $1 \times 10^{-11}$  or even below, approaching the SM prediction [23].

We predict the branching ratio  $\mathcal{B}(K_S^0 \rightarrow \mu^+ \mu^-)$  under consideration of MSSM contributions and taking into account the relevant experimental constraints on the branching fractions  $\mathcal{B}(K_L^0 \rightarrow \mu^+ \mu^-)$ ,  $\mathcal{B}(B^+ \rightarrow \tau^+ \nu_\tau)$  and  $\mathcal{B}(K^+ \rightarrow \mu^+ \nu_\mu)$ , the  $CP$  violation parameters  $\varepsilon'_K / \varepsilon_K$  and  $\varepsilon_K$ , the  $K_L^0 - K_S^0$  mass difference,  $\Delta M_K \equiv M_{K_L^0} - M_{K_S^0} > 0$ , and the Wilson coefficient  $C_7$  from  $b \rightarrow s \gamma$ . We use the Mass Insertion Approximation (MIA) [24], treating the mass insertion terms as phenomenological parameters at the SUSY scale. The details of the formalism are given in section 2. The subsets of the MSSM parameter space are studied in scans performed on Graphics Processing Units (GPU), as detailed in section 3. The results are shown in section 4 and conclusions are drawn in section 5.

## 2 Formalism

### 2.1 Definitions

In this paper, we follow the notations of refs. [25, 26]. We denote the right-handed down and up squarks as  $D$  and  $U$ . On the other hand, the two left-handed squarks have the

<sup>1</sup>Note that this enhancement factor is not present in the up-type quark case.

<sup>2</sup>The higher-order contributions have been derived up to two-loop level in refs. [7–9].

same mass because of the  $SU(2)_L$  doublet, and they are denoted as  $Q$ . The average of the  $Q$ ,  $D$ , and  $U$ -squark masses squared are denoted by  $\tilde{m}_Q^2$ ,  $\tilde{m}_d^2$ ,  $\tilde{m}_u^2$ , respectively.

The mass insertions (hereafter MIs) are defined as:

$$(\delta_d^{LL})_{ij} = \frac{[(\mathcal{M}_D^2)_{LL}]_{ij}}{\tilde{m}_Q^2} = \frac{(m_Q^2)_{ji}}{\tilde{m}_Q^2}, \quad (2.1)$$

$$(\delta_u^{LL})_{ij} = \frac{[(\mathcal{M}_U^2)_{LL}]_{ij}}{\tilde{m}_Q^2} = \frac{(Vm_Q^2 V^\dagger)_{ji}}{\tilde{m}_Q^2}, \quad (2.2)$$

$$(\delta_d^{RR})_{ij} = \frac{[(\mathcal{M}_D^2)_{RR}]_{ij}}{\tilde{m}_d^2} = \frac{(m_D^2)_{ij}}{\tilde{m}_d^2}, \quad (2.3)$$

where  $V$  is the Cabibbo-Kobayashi-Maskawa (CKM) matrix and  $\mathcal{M}_{D,U}^2$  are the  $6 \times 6$  squark mass matrices. Note that the indices  $ij$  are inverted for  $LL$ . Comparison with the SUSY Les Houches Accord 2 convention [27] is given in the appendix of ref. [25].

The running coupling constants  $\alpha_1$ ,  $\alpha_2$ , and  $\alpha_3$  are defined as

$$\alpha_1 = \frac{g_1^2}{4\pi} = \frac{5}{3} \frac{g'^2}{4\pi}, \quad (2.4)$$

$$\alpha_2 = \frac{g_2^2}{4\pi} = \frac{g^2}{4\pi}, \quad (2.5)$$

$$\alpha_3 = \frac{g_3^2}{4\pi} = \frac{g_s^2}{4\pi}, \quad (2.6)$$

where  $g'$ ,  $g$ , and  $g_s$  are the  $U(1)_Y$ ,  $SU(2)_L$ , and  $SU(3)_C$  group coupling constants, respectively. In the following, these couplings are evaluated at the  $\mu^{\text{SUSY}}$  scale, where we define  $\mu^{\text{SUSY}} = \sqrt{\tilde{m}_Q M_3}$ .

## 2.2 Observables

As will be shown in the next subsections, the main MSSM contribution to  $\mathcal{B}(K_S^0 \rightarrow \mu^+ \mu^-)$  is proportional to  $\left[ \left( \delta_d^{LL(RR)} \right)_{12} \mu \tan^3 \beta M_3 / M_A^2 \right]^2$ . In order to constrain those parameters, the following observables are calculated in addition to  $\mathcal{B}(K_S^0 \rightarrow \mu^+ \mu^-)$ :

- Observables sensitive, among others, to the off-diagonal mass insertion terms  $\left( \delta_d^{LL(RR)} \right)_{12} : \mathcal{B}(K_L^0 \rightarrow \mu^+ \mu^-)$ ,  $\varepsilon'_K / \varepsilon_K$ ,  $\varepsilon_K$ , and  $\Delta M_K$ .<sup>3</sup>
- Observables sensitive to  $\tan \beta$  and the heavy Higgs mass:  $\mathcal{B}(B^+ \rightarrow \tau^+ \nu_\tau)$ ,  $\mathcal{B}(K^+ \rightarrow \mu^+ \nu_\mu)$ ,  $\Delta C_7$ .

The definitions of  $\mathcal{B}(B^+ \rightarrow \tau^+ \nu_\tau)$ ,  $\mathcal{B}(K^+ \rightarrow \mu^+ \nu_\mu)$ , and  $C_7$  are given in ref. [25] and the remaining observables are defined in the following subsections. The CKM matrix is fitted excluding measurements with potential sensitivity to MSSM contributions.

The constraints we impose on physics observables sensitive to the MSSM same parameters as  $\mathcal{B}(K_S^0 \rightarrow \mu^+ \mu^-)$  are listed in table 1, where the EXP/SM represents the measured

<sup>3</sup>The contributions to  $\mathcal{B}(K \rightarrow \pi \nu \bar{\nu})$  are controlled by an additional free parameter, the slepton mass, and  $\mathcal{O}(1)$  effects are possible in this scenario [28].

Observable	Constraint
$\mathcal{B}(K_S^0 \rightarrow \mu^+ \mu^-)^{\text{EXP/SM}}$	unconstrained
$\mathcal{B}(K_L^0 \rightarrow \mu^+ \mu^-)^{\text{EXP/SM}}$	$1.00 \pm 0.12$ (+) [21, 36, 37]
	$0.84 \pm 0.16$ (-) [21, 36, 37]
$\Delta M_K^{\text{EXP/SM}}$	$1 \pm 1$
$\varepsilon_K^{\text{EXP/SM}}$	$1.05 \pm 0.10$ [37–39]
$\Delta(\varepsilon'_K/\varepsilon_K)^{\text{EXP-SM}}$	$[15.5 \pm 2.3(\text{EXP}) \pm 5.07(\text{TH})] \times 10^{-4}$ [37, 40]
$\mathcal{B}(B^+ \rightarrow \tau^+ \nu_\tau)^{\text{EXP/SM}}$	$0.91 \pm 0.22$ [37]
$\mathcal{B}(K^+ \rightarrow \mu^+ \nu_\mu)^{\text{EXP/SM}}$	$1.0004 \pm 0.0095$ [37]
$\Delta C_7$	$-0.02 \pm 0.02$ [41]
$\tan \beta: M_A$ plane	ATLAS limits for hMSSM scenario [42]
LSP	Lightest neutralino
$B_G$	$1 \pm 3(\text{TH})$ [43, 44]

**Table 1.** Physics observables constraints imposed in this study. The two different constraints on  $\mathcal{B}(K_L^0 \rightarrow \mu^+ \mu^-)^{\text{EXP/SM}}$  arise from an unknown sign of  $A_{L\gamma\gamma}^\mu$  in eq. (2.16) (see refs. [21, 36]).

value over the SM prediction with their uncertainties. Due to the poor theoretical knowledge of  $\Delta M_K$ , we assign a 100% theoretical uncertainty; thus, the constraint imposed on this observable penalizes only  $\mathcal{O}(1)$  effects. It is not counted as a degree of freedom in the  $\chi^2$  tests, so that the  $\Delta M_K$  constraint can only make the bounds tighter, but never looser. Remaining constraints can in principle be satisfied by adjusting the other parameters of the model. In particular,  $B$  physics constraints not included in our list can be satisfied by parameters unspecified in our scan, for example by setting  $\delta_{13} \approx \delta_{23} \approx 0$  and small  $A_t$ . The relation of eq. (2.2) may induce non-zero up-type MIs in the  $B$  sector and hence modify  $B_{s(d)}^0 \rightarrow \mu^+ \mu^-$ , however, we checked that these effects can be safely neglected in the scenarios we studied. The large SUSY masses in our scan are typically beyond the reach of LHC.

The lattice values for  $(\varepsilon'_K/\varepsilon_K)^{\text{SM}}$  used are from refs. [29–32], although the conclusions of our study remain largely unchanged if we use the  $\chi_{PT}$  value from refs. [33–35] instead. The values of  $\varepsilon_K^{\text{EXP/SM}}$  and  $\Delta(\varepsilon'_K/\varepsilon_K)^{\text{EXP-SM}}$  are discussed in more detail in the following subsections.

### 2.3 $K^0 \rightarrow \mu^+ \mu^-$

The  $|\Delta S| = 1$  effective Hamiltonian relevant for the  $K^0 \rightarrow \ell\bar{\ell}$  transition at the  $Z$  boson mass scale is

$$\mathcal{H}_{\text{eff}} = -C_A Q_A - \tilde{C}_A \tilde{Q}_A - C_S Q_S - \tilde{C}_S \tilde{Q}_S - C_P Q_P - \tilde{C}_P \tilde{Q}_P + \text{H.c.}, \quad (2.7)$$

where  $C_A$ ,  $C_S$  and  $C_P$  are the axial, scalar and pseudoscalar Wilson coefficients. The right-handed and left-handed axial ( $\tilde{Q}_A, Q_A$ ), scalar ( $Q_S, \tilde{Q}_S$ ) and pseudoscalar ( $Q_P, \tilde{Q}_P$ )

operators are given by:

$$\begin{aligned}
 Q_A &= (\bar{s}\gamma^\mu P_L d)(\bar{\ell}\gamma_\mu\gamma_5\ell), & \tilde{Q}_A &= (\bar{s}\gamma^\mu P_R d)(\bar{\ell}\gamma_\mu\gamma_5\ell), \\
 Q_S &= m_s(\bar{s}P_R d)(\bar{\ell}\ell), & \tilde{Q}_S &= m_s(\bar{s}P_L d)(\bar{\ell}\ell), \\
 Q_P &= m_s(\bar{s}P_R d)(\bar{\ell}\gamma_5\ell), & \tilde{Q}_P &= m_s(\bar{s}P_L d)(\bar{\ell}\gamma_5\ell),
 \end{aligned}
 \tag{2.8}$$

where  $P_{L,R}$  are the left and right-handed projection operators. For  $\mathcal{B}(K_{S,L}^0 \rightarrow \mu^+\mu^-)$ ,<sup>4</sup> there are two contributions from S-wave ( $A_{S,L}$ ) and P-wave transitions ( $B_{S,L}$ ), resulting in:<sup>5</sup>

$$\mathcal{B}(K_{S,L}^0 \rightarrow \mu^+\mu^-) = \tau_{S,L}\Gamma(K_{S,L}^0 \rightarrow \mu^+\mu^-) = \tau_{S,L}\frac{f_K^2 M_K^3 \beta_\mu}{16\pi} (|A_{S,L}|^2 + \beta_\mu^2 |B_{S,L}|^2), \tag{2.9}$$

with

$$A_S = \frac{m_s M_K}{m_s + m_d} \text{Im}(C_P - \tilde{C}_P) + \frac{2m_\mu}{M_K} \text{Im}(C_A - \tilde{C}_A), \tag{2.10}$$

$$B_S = \frac{2G_F^2 M_W^2 m_\mu}{\pi^2 M_K} B_{S\gamma\gamma}^\mu - \frac{m_s M_K}{m_s + m_d} \text{Re}(C_S - \tilde{C}_S), \tag{2.11}$$

and

$$A_L = \frac{2G_F^2 M_W^2 m_\mu}{\pi^2 M_K} A_{L\gamma\gamma}^\mu - \frac{m_s M_K}{m_s + m_d} \text{Re}(C_P - \tilde{C}_P) - \frac{2m_\mu}{M_K} \text{Re}(C_A - \tilde{C}_A), \tag{2.12}$$

$$B_L = \frac{m_s M_K}{m_s + m_d} \text{Im}(C_S - \tilde{C}_S), \tag{2.13}$$

where

$$\beta_\mu = \sqrt{1 - \frac{4m_\mu^2}{M_K^2}}. \tag{2.14}$$

Here, the long-distance contributions are [19–21, 45]:

$$\frac{2G_F^2 M_W^2 m_\mu}{\pi^2 M_K} B_{S\gamma\gamma}^\mu = (-2.65 + 1.14i) \times 10^{-11} (\text{GeV})^{-2}, \tag{2.15}$$

$$\frac{2G_F^2 M_W^2 m_\mu}{\pi^2 M_K} A_{L\gamma\gamma}^\mu = \pm(0.54 - 3.96i) \times 10^{-11} (\text{GeV})^{-2}, \tag{2.16}$$

with<sup>6</sup>

$$B_{S\gamma\gamma}^\mu = \frac{\pi\alpha_0}{G_F^2 M_W^2 f_K M_K |H(0)|} \mathcal{I}\left(\frac{m_\mu^2}{M_K^2}, \frac{m_{\pi^\pm}^2}{M_K^2}\right) \sqrt{\frac{2\pi}{M_K} \frac{\mathcal{B}(K_S^0 \rightarrow \gamma\gamma)^{\text{EXP}}}{\tau_S}}, \tag{2.17}$$

$$A_{L\gamma\gamma}^\mu = \frac{\pm 2\pi\alpha_0}{G_F^2 M_W^2 f_K M_K} \mathcal{A}(M_K^2) \sqrt{\frac{2\pi}{M_K} \frac{\mathcal{B}(K_L^0 \rightarrow \gamma\gamma)^{\text{EXP}}}{\tau_L}}, \tag{2.18}$$

<sup>4</sup>The electron modes are suppressed by  $m_e^2/m_\mu^2$ , and we do not consider them in this paper.

<sup>5</sup>Our result agrees with refs. [45–48]. However, it disagrees with notable literature [6, 25] after discarding the long-distance contributions. We found that  $C_{10}^{\text{SM}}$  should be  $-C_{10}^{\text{SM}}$  in eq. (3.45) of ref. [25], and  $(C_P - C'_P)$  should be  $(C'_P - C_P)$  in eq. (2.4) of ref. [6].

<sup>6</sup>Note that  $B_{S\gamma\gamma}^\mu$  is denoted by  $A_{S\gamma\gamma}^\mu$  in refs. [21, 45].

where a two-loop function  $\mathcal{I}(a, b)$  from the  $2\pi^\pm 2\gamma$  intermediate state is given in refs. [19, 49], a pion one-loop contribution with two external on-shell photons is represented as  $H(0) = 0.331 + i0.583$  [19], and a one-loop function  $\mathcal{A}(s)$  from the  $2\gamma$  intermediate state is given in refs. [50, 51]. Here,  $\alpha_0 = 1/137.04$ ,  $f_K = (155.9 \pm 0.4) \text{ MeV}$  [37], and  $\tau_{S,L}$  are the  $K_{S,L}^0$  lifetimes. Note that there is a theoretically and experimentally unknown sign in  $A_{L\gamma\gamma}^\mu$ , which is determined by higher chiral orders than  $\mathcal{O}(p^4)$  contributions [52, 53], and they provide two different constraints on  $\mathcal{B}(K_L^0 \rightarrow \mu^+\mu^-)^{\text{EXP/SM}}$  in table 1. This sign can be determined by a precise measurement of the interference between  $K_L^0 \rightarrow \mu^+\mu^-$  and  $K_S^0 \rightarrow \mu^+\mu^-$  [21]. In addition, in the MSSM, the correlation between  $\mathcal{B}(K_S^0 \rightarrow \mu^+\mu^-)$  and  $\mathcal{B}(K_L^0 \rightarrow \mu^+\mu^-)$  depends on the unknown sign of  $A_{L\gamma\gamma}^\mu$ . In the following, we derive some relations between the two branching fractions, for a better interpretation of the results of our scans. In the case in which new physics enters only in  $\tilde{C}_S$  and  $\tilde{C}_P = \tilde{C}_S$  (pure left-handed MSSM scenario), the following relations between the branching fractions of  $K_S^0$  and  $K_L^0$  decaying into  $\mu^+\mu^-$  can be established:

$$\begin{aligned} \mathcal{B}(K_S^0 \rightarrow \mu^+\mu^-) &\propto \beta_\mu^2 |N_S^{\text{LD}}|^2 + (A_{S,\text{SM}}^{\text{SD}})^2 - 2M_K \left[ A_{S,\text{SM}}^{\text{SD}} \text{Im}(\tilde{C}_S) - \beta_\mu^2 \text{Re}(N_S^{\text{LD}}) \text{Re}(\tilde{C}_S) \right] \\ &\quad + M_K^2 \left\{ [\text{Im}(\tilde{C}_S)]^2 + \beta_\mu^2 [\text{Re}(\tilde{C}_S)]^2 \right\}, \end{aligned} \quad (2.19)$$

$$\begin{aligned} \mathcal{B}(K_L^0 \rightarrow \mu^+\mu^-) &\propto |N_L^{\text{LD}}|^2 + (A_{L,\text{SM}}^{\text{SD}})^2 - 2M_K \text{Re}(\tilde{C}_S) [A_{L,\text{SM}}^{\text{SD}} - \text{Re}(N_L^{\text{LD}})] \\ &\quad + M_K^2 \left\{ [\text{Re}(\tilde{C}_S)]^2 + \beta_\mu^2 [\text{Im}(\tilde{C}_S)]^2 \right\} - 2A_{L,\text{SM}}^{\text{SD}} \text{Re}(N_L^{\text{LD}}), \end{aligned} \quad (2.20)$$

with

$$A_{S,\text{SM}}^{\text{SD}} = \frac{2m_\mu}{M_K} \text{Im}(C_{A,\text{SM}}), \quad A_{L,\text{SM}}^{\text{SD}} = \frac{2m_\mu}{M_K} \text{Re}(C_{A,\text{SM}}), \quad (2.21)$$

and

$$N_S^{\text{LD}} = \frac{2G_F^2 M_W^2 m_\mu}{\pi^2 M_K} B_{S\gamma\gamma}^\mu, \quad N_L^{\text{LD}} = \frac{2G_F^2 M_W^2 m_\mu}{\pi^2 M_K} A_{L\gamma\gamma}^\mu, \quad (2.22)$$

where  $m_d$  terms are discarded for simplicity. The long-distance term  $\text{Re}(N_L^{\text{LD}})$  holds the unknown sign from  $A_{L\gamma\gamma}^\mu$ , which changes the correlation significantly, as will be shown. On the other hand, if new physics produces only  $C_S$  and  $C_P = -C_S$  (pure right-handed MSSM), the two branching fractions are

$$\begin{aligned} \mathcal{B}(K_S^0 \rightarrow \mu^+\mu^-) &\propto \beta_\mu^2 |N_S^{\text{LD}}|^2 + (A_{S,\text{SM}}^{\text{SD}})^2 - 2M_K [A_{S,\text{SM}}^{\text{SD}} \text{Im}(C_S) + \beta_\mu^2 \text{Re}(N_S^{\text{LD}}) \text{Re}(C_S)] \\ &\quad + M_K^2 \left\{ [\text{Im}(C_S)]^2 + \beta_\mu^2 [\text{Re}(C_S)]^2 \right\}, \end{aligned} \quad (2.23)$$

$$\begin{aligned} \mathcal{B}(K_L^0 \rightarrow \mu^+\mu^-) &\propto |N_L^{\text{LD}}|^2 + (A_{L,\text{SM}}^{\text{SD}})^2 - 2M_K \text{Re}(C_S) [A_{L,\text{SM}}^{\text{SD}} - \text{Re}(N_L^{\text{LD}})] \\ &\quad + M_K^2 \left\{ [\text{Re}(C_S)]^2 + \beta_\mu^2 [\text{Im}(C_S)]^2 \right\} - 2A_{L,\text{SM}}^{\text{SD}} \text{Re}(N_L^{\text{LD}}). \end{aligned} \quad (2.24)$$

It is shown that  $\mathcal{B}(K_L^0 \rightarrow \mu^+\mu^-)$  is the same as the pure left-handed one by a replacement of  $C_S \rightarrow \tilde{C}_S$ , while  $\mathcal{B}(K_S^0 \rightarrow \mu^+\mu^-)$  is not; the final terms of the first line have opposite

sign. Hence, the relations between the two branching fractions are different for left-handed and right-handed new physics scenarios.

For those cases, the experimental measurement of  $\mathcal{B}(K_L^0 \rightarrow \mu^+\mu^-)$  [37],

$$\mathcal{B}(K_L^0 \rightarrow \mu^+\mu^-)^{\text{EXP}} = (6.84 \pm 0.11) \times 10^{-9}, \quad (2.25)$$

imposes an upper bound on  $\mathcal{B}(K_S^0 \rightarrow \mu^+\mu^-)$ . This bound can be alleviated if  $|C_S| \neq |C_P|$  or if new physics is present simultaneously in the left-handed and right-handed Wilson coefficients.

Experimentally, one can also access an *effective* branching ratio of  $K_S^0 \rightarrow \mu^+\mu^-$  [21] which includes an interference contribution with  $K_L^0 \rightarrow \mu^+\mu^-$  in the neutral kaon sample. We obtain

$$\begin{aligned} \mathcal{B}(K_S^0 \rightarrow \mu^+\mu^-)_{\text{eff}} = \tau_S \left( \int_{t_{\min}}^{t_{\max}} dt e^{-\Gamma_S t} \varepsilon(t) \right)^{-1} \left[ \int_{t_{\min}}^{t_{\max}} dt \left\{ \Gamma(K_S^0 \rightarrow \mu^+\mu^-) e^{-\Gamma_S t} \right. \right. \\ \left. \left. + \frac{D f_K^2 M_K^3 \beta_\mu}{8\pi} \text{Re} [i (A_S A_L - \beta_\mu^2 B_S^* B_L) e^{-i\Delta M_K t}] e^{-\frac{\Gamma_S + \Gamma_L}{2} t} \right\} \varepsilon(t) \right], \end{aligned} \quad (2.26)$$

where the dilution factor  $D$  is a measure of the initial ( $t = 0$ )  $K^0 - \bar{K}^0$  asymmetry,

$$D = \frac{K^0 - \bar{K}^0}{K^0 + \bar{K}^0}, \quad (2.27)$$

$\varepsilon(t)$  is the decay-time acceptance of the detector. The second line of eq. (2.26) corresponds to an interference effect between  $K_L^0$  and  $K_S^0$ , and for  $D = 0$ ,  $\mathcal{B}(K_S^0 \rightarrow \mu^+\mu^-)_{\text{eff}}$  corresponds to  $\mathcal{B}(K_S^0 \rightarrow \mu^+\mu^-)$ . The current experimental bound [22],

$$\mathcal{B}(K_S^0 \rightarrow \mu^+\mu^-)^{\text{EXP}} < 8 \times 10^{-10} \text{ [90\% C.L.]}, \quad (2.28)$$

uses untagged  $K^0$  and  $\bar{K}^0$  mesons produced in almost equal amounts, and hence  $D = 0$  is assumed. A pure  $K_L^0 \rightarrow \mu^+\mu^-$  background can be subtracted by a combination of simultaneous measurement of  $K_S^0 \rightarrow \pi^+\pi^-$  events and knowledge of the observed value of  $\mathcal{B}(K_L^0 \rightarrow \mu^+\mu^-)$  in eq. (2.25) [21]. The decay-time acceptance of the LHCb detector is parametrized by  $\varepsilon(t) = \exp(-\beta t)$  with  $\beta \simeq 86 \text{ ns}^{-1}$ , and the range of the detector for selecting  $K^0 \rightarrow \mu^+\mu^-$  is  $t_{\min} = 8.95 \text{ ps} = 0.1\tau_S$  and  $t_{\max} = 130 \text{ ps} = 1.45\tau_S$ .

Given the potential measurement of an effective branching ratio by different dilution factors  $D > 0$  and  $D' < 0$  using  $K^-$  tagging and  $K^+$  tagging [21], respectively, the direct  $CP$  asymmetry can be measured using the difference  $\mathcal{B}(K_S^0 \rightarrow \mu^+\mu^-)_{\text{eff}}(D) - \mathcal{B}(K_S^0 \rightarrow \mu^+\mu^-)_{\text{eff}}(D')$ , which is a theoretically clean quantity that emerges from a genuine direct  $CP$  violation. Here, the charged kaon is accompanied by the neutral kaon beam as, for instance,  $pp \rightarrow K^0 K^- X$  or  $pp \rightarrow \bar{K}^0 K^+ X$ . Note that a definition of  $D'$  is the same as  $D$  in eq. (2.27) but charged kaons of opposite sign are required in the event selection. Therefore, we define the following direct  $CP$  asymmetry in  $K_S^0 \rightarrow \mu^+\mu^-$ :

$$A_{CP}(K_S^0 \rightarrow \mu^+\mu^-)_{D,D'} = \frac{\mathcal{B}(K_S^0 \rightarrow \mu^+\mu^-)_{\text{eff}}(D) - \mathcal{B}(K_S^0 \rightarrow \mu^+\mu^-)_{\text{eff}}(D')}{\mathcal{B}(K_S^0 \rightarrow \mu^+\mu^-)_{\text{eff}}(D) + \mathcal{B}(K_S^0 \rightarrow \mu^+\mu^-)_{\text{eff}}(D')}. \quad (2.29)$$



We discarded the indirect  $CP$ -violating contributions because they are numerically negligible compared to the  $CP$ -conserving and the direct  $CP$ -violating contributions [21].

Within the SM, the Wilson coefficients are,

$$C_{A,\text{SM}} = -\frac{[\alpha_2(M_Z)]^2}{2M_W^2} (V_{ts}^* V_{td} Y_t + V_{cs}^* V_{cd} Y_c), \quad (2.30)$$

$$\tilde{C}_{A,\text{SM}} = C_{S,\text{SM}} = \tilde{C}_{S,\text{SM}} = C_{P,\text{SM}} = \tilde{C}_{P,\text{SM}} \simeq 0, \quad (2.31)$$

where  $Y_t = 0.950 \pm 0.049$  and  $Y_c = (2.95 \pm 0.46) \times 10^{-4}$  [54]. Using the CKM matrix tailored for probing the MSSM contributions, we obtain the SM prediction of  $A_{CP}$ ,

$$A_{CP}(K_S^0 \rightarrow \mu^+ \mu^-)_{D,D'}^{\text{SM}} = \begin{cases} -\frac{3.71(D-D')}{(10.53 \pm 3.01) - 3.71(D+D')}, & (+) \\ \frac{3.98(D-D')}{(10.53 \pm 3.01) + 3.98(D+D')}, & (-) \end{cases} \quad (2.32)$$

where (+) and (-) correspond to the unknown sign of  $A_{L\gamma\gamma}^\mu$  in eq. (2.16). The uncertainty is totally dominated by  $B_{S\gamma\gamma}^\mu$  [21] and it will be sharpened by the dispersive treatment of  $K_S^0 \rightarrow \gamma^{(*)}\gamma^{(*)}$  [55]. If one considers the case of  $D' = -D$  achieved by the accompanying opposite-charged-kaon tagging, the SM prediction of  $A_{CP}$  is simplified:

$$A_{CP}(K_S^0 \rightarrow \mu^+ \mu^-)_{D,-D}^{\text{SM}} = \begin{cases} (-0.704_{-0.281}^{+0.156}) \times D, & (+) \\ (+0.756_{-0.168}^{+0.302}) \times D. & (-) \end{cases} \quad (2.33)$$

In the MSSM, the leading contribution to  $C_A$ , induced by terms of second order in the expansion of the squark mass matrix of the chargino  $Z$ -penguin, is [6, 56],

$$C_A = -\frac{(\alpha_2)^2}{16M_W^2} \frac{[(\mathcal{M}_U^2)_{LR}]_{23}^* [(\mathcal{M}_U^2)_{LR}]_{13}}{M_A^4} l(x_2^Q, x_2^u), \quad (2.34)$$

$$\tilde{C}_A = 0, \quad (2.35)$$

where  $x_2^Q = \tilde{m}_Q^2/M_2^2$  and  $x_2^u = \tilde{m}_u^2/M_2^2$ . The loop function  $l(x, y)$  [56] is defined in appendix B.1. Here, contributions from the Wino-Higgsino mixing are omitted. Setting  $\tilde{m}_Q^2 = \tilde{m}_u^2$  gives the MIA result of refs. [43, 57].

The leading MSSM contributions to  $C_{S(P)}$  and  $\tilde{C}_{S(P)}$  in  $K_S^0 \rightarrow \mu^+ \mu^-$  and  $K_L^0 \rightarrow \mu^+ \mu^-$  are shown in figure 1. For  $C_S$  and  $\tilde{C}_S$ , we obtain

$$\begin{aligned} C_S &= -\frac{2}{3} \frac{\alpha_s \alpha_2 m_\mu}{M_W^2} \frac{\mu M_3}{M_A^2 \tilde{m}_d^2} (\delta_d^{RR})_{12} \frac{\tan^3 \beta}{(1 + \epsilon_g \tan \beta)^2 (1 + \epsilon_\ell \tan \beta)} G(x_d^3, x_d^Q) \\ &\quad - \frac{2}{3} \frac{\alpha_s \alpha_2 m_\mu}{M_W^2} \frac{m_b}{m_s} \frac{\mu M_3 \tilde{m}_Q^2}{M_A^2 \tilde{m}_d^4} (\delta_d^{RR})_{13} (\delta_d^{LL})_{32} \\ &\quad \times \frac{\tan^3 \beta}{(1 + \epsilon_g \tan \beta)[1 + (\epsilon_g + \epsilon_Y y_t^2) \tan \beta](1 + \epsilon_\ell \tan \beta)} H(x_d^3, x_d^Q), \quad (2.36) \\ \tilde{C}_S &= -\frac{2}{3} \frac{\alpha_s \alpha_2 m_\mu}{M_W^2} \frac{\mu M_3}{M_A^2 \tilde{m}_Q^2} (\delta_d^{LL})_{12} \frac{\tan^3 \beta}{(1 + \epsilon_g \tan \beta)^2 (1 + \epsilon_\ell \tan \beta)} G(x_Q^3, x_Q^d) \\ &\quad - \frac{2}{3} \frac{\alpha_s \alpha_2 m_\mu}{M_W^2} \frac{m_b}{m_s} \frac{\mu M_3 \tilde{m}_d^2}{M_A^2 \tilde{m}_Q^4} (\delta_d^{LL})_{13} (\delta_d^{RR})_{32} \end{aligned}$$

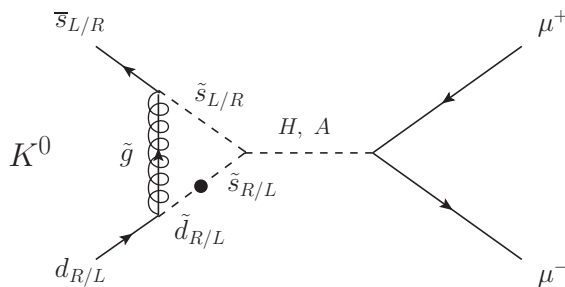


**Figure 1.** Feynman diagram of the leading (pseudo-)scalar MSSM contributions to  $K_S^0 \rightarrow \mu^+\mu^-$  and  $K_L^0 \rightarrow \mu^+\mu^-$ , which include a gluino and a heavy Higgs boson. The black dot is the corresponding mass insertion term.

$$\begin{aligned}
 & \times \frac{\tan^3 \beta}{(1 + \epsilon_g \tan \beta)[1 + (\epsilon_g + \epsilon_Y y_t^2) \tan \beta](1 + \epsilon_\ell \tan \beta)} H(x_Q^3, x_Q^d) \\
 & + \frac{(\alpha_2)^2 m_\mu m_t^2}{8M_W^4} \frac{\mu A_t}{M_A^2 \tilde{m}_Q^2} V_{ts}^* V_{td} \frac{\tan^3 \beta [1 + (\epsilon_g + \epsilon_Y y_t^2) \tan \beta]^2}{(1 + \epsilon_g \tan \beta)^4 (1 + \epsilon_\ell \tan \beta)} F(x_Q^\mu, x_Q^u) \\
 & + \frac{(\alpha_2)^2 m_\mu}{4M_W^2} \frac{\mu M_2}{M_A^2 \tilde{m}_Q^2} (\delta_u^{LL})_{12} \frac{\tan^3 \beta}{(1 + \epsilon_g \tan \beta)^2 (1 + \epsilon_\ell \tan \beta)} G(x_Q^2, x_Q^\mu), \quad (2.37)
 \end{aligned}$$

with

$$\epsilon_g = \frac{2\alpha_s}{3\pi} \frac{\mu M_3}{\tilde{m}_Q^2} F(x_Q^3, x_Q^d), \quad (2.38)$$

$$\epsilon_Y = \frac{1}{16\pi} \frac{\mu A_t}{\tilde{m}_Q^2} F(x_Q^\mu, x_Q^u), \quad (2.39)$$

$$\epsilon_\ell \simeq -\frac{3\alpha_2}{16\pi}, \quad (2.40)$$

where  $x_d^3 = M_3^2/\tilde{m}_d^2$ ,  $x_d^Q = \tilde{m}_Q^2/\tilde{m}_d^2$ ,  $x_Q^3 = M_3^2/\tilde{m}_Q^2$ ,  $x_Q^d = \tilde{m}_d^2/\tilde{m}_Q^2$ ,  $x_Q^\mu = \mu^2/\tilde{m}_Q^2$ ,  $x_Q^u = \tilde{m}_u^2/\tilde{m}_Q^2$ ,  $x_Q^2 = M_2^2/\tilde{m}_Q^2$ , and  $x_Q^\mu = \mu^2/\tilde{m}_Q^2$ . The loop functions  $F(x, y)$ ,  $G(x, y)$ , and  $H(x, y)$  are defined in appendix B.1. These results are consistent with ref. [25] in the universal squark mass limit after changing the flavour and its chirality for  $B_s^0$  decay. Here, we used the following approximation

$$\alpha \simeq \beta - \frac{\pi}{2}, \quad M_H \simeq M_A, \quad (2.41)$$

where  $\alpha$  is an angle of the orthogonal rotation matrix for the  $CP$ -even Higgs mass, and  $M_H$  ( $M_A$ ) is a  $CP$ -even (odd) heavy Higgs mass. On the other hand, the contributions to  $C_P$  and  $\tilde{C}_P$  are

$$C_P = -C_S, \quad \tilde{C}_P = \tilde{C}_S. \quad (2.42)$$

Note that the Wilson coefficients in the MSSM are given at the  $\mu^{\text{SUSY}}$  scale, and there is no QCD correction from the renormalization-group (RG) evolution at the leading order.

## 2.4 $\varepsilon'_K/\varepsilon_K$

New physics models affecting  $\varepsilon'_K/\varepsilon_K$  have recently attracted some attention since lattice results from the RBC and UKQCD collaborations [29–32] have been reported 2–3 $\sigma$  below [40, 58] the experimental world average of  $\text{Re}(\varepsilon'_K/\varepsilon_K)$  [37]. This is consistent with the recent calculations in the large- $N_c$  analyses [59, 60]. Although the lattice simulation [32] includes final-state interactions partially along the line of ref. [61], final-state interactions have to be still fully included in the calculations in light of a discrepancy of a strong phase shift  $\delta_0$  [62–64]. Conversely combining large- $N_c$  methods with chiral loop corrections can bring the value of  $\varepsilon'_K/\varepsilon_K$  in agreement with the experiment [33–35].

In this paper, we used the hadronic matrix elements obtained by lattice simulations. For the  $\chi^2$  test, we use the following constraint,

$$\Delta \left( \frac{\varepsilon'_K}{\varepsilon_K} \right)^{\text{EXP-SM}} \equiv \text{Re} \left( \frac{\varepsilon'_K}{\varepsilon_K} \right)^{\text{EXP}} - \left( \frac{\varepsilon'_K}{\varepsilon_K} \right)^{\text{SM}} = [15.5 \pm 2.3(\text{EXP}) \pm 5.07(\text{TH})] \times 10^{-4}, \quad (2.43)$$

with

$$\left( \frac{\varepsilon'_K}{\varepsilon_K} \right)^{\text{SM}} \rightarrow \left( \frac{\varepsilon'_K}{\varepsilon_K} \right)^{\text{SM}} + \left( \frac{\varepsilon'_K}{\varepsilon_K} \right)^{\text{SUSY}}, \quad (2.44)$$

where the SM prediction at the next-to-leading order in ref. [40] is used. The experimental value of  $\varepsilon_K$  is used in the calculation of the ratio. The SUSY contributions to  $\varepsilon_K$  are given in the next subsection.

Within the MSSM, the SUSY contributions to  $\varepsilon'_K/\varepsilon_K$  are dominated by gluino box, chargino-mediated  $Z$ -penguin, and chromomagnetic dipole contributions. The first two contributions are represented by the same  $|\Delta S| = 1$  four-quark effective Hamiltonian at the  $\mu^{\text{SUSY}}$  scale, which is:

$$\mathcal{H}_{\text{eff}} = \frac{G_F}{\sqrt{2}} \sum_q \sum_{i=1}^4 \left[ C_i^q Q_i^q + \tilde{C}_i^q \tilde{Q}_i^q \right] + \text{H.c.}, \quad (2.45)$$

with

$$\begin{aligned} Q_1^q &= (\bar{s}d)_{V-A} (\bar{q}q)_{V+A}, & \tilde{Q}_1^q &= (\bar{s}d)_{V+A} (\bar{q}q)_{V-A}, \\ Q_2^q &= (\bar{s}_\alpha d_\beta)_{V-A} (\bar{q}_\beta q_\alpha)_{V+A}, & \tilde{Q}_2^q &= (\bar{s}_\alpha d_\beta)_{V+A} (\bar{q}_\beta q_\alpha)_{V-A}, \\ Q_3^q &= (\bar{s}d)_{V-A} (\bar{q}q)_{V-A}, & \tilde{Q}_3^q &= (\bar{s}d)_{V+A} (\bar{q}q)_{V+A}, \\ Q_4^q &= (\bar{s}_\alpha d_\beta)_{V-A} (\bar{q}_\beta q_\alpha)_{V-A}, & \tilde{Q}_4^q &= (\bar{s}_\alpha d_\beta)_{V+A} (\bar{q}_\beta q_\alpha)_{V+A}, \end{aligned} \quad (2.46)$$

where  $(V \mp A)$  refers to  $\gamma_\mu(1 \mp \gamma_5)$ , and  $\alpha$  and  $\beta$  are color indices.

The Wilson coefficients from the gluino box contributions are leading contributions when the mass difference between right-handed squarks exists [65, 66]. They are shown in appendix A.1 with their corresponding loop functions defined in appendix B.2.1. Here,  $(\delta_d)_{13}(\delta_d)_{32}$  terms are discarded for simplicity.

The Wilson coefficients of the chargino-mediated  $Z$ -penguin are induced by terms of second order in the expansion of MIA. These ones are shown in appendix A.2, where the loop function  $l(x, y)$  is given by eq. (B.1).

The matching conditions to the standard four-quark Wilson coefficients [40] are

$$\begin{aligned}
 s_1 &= 0, & s_2 &= 0, \\
 s_3 &= \frac{1}{3} (C_3^u + 2C_3^d), & s_4 &= \frac{1}{3} (C_4^u + 2C_4^d), \\
 s_5 &= \frac{1}{3} (C_1^u + 2C_1^d), & s_6 &= \frac{1}{3} (C_2^u + 2C_2^d), \\
 s_7 &= \frac{2}{3} (C_1^u - C_1^d), & s_8 &= \frac{2}{3} (C_2^u - C_2^d), \\
 s_9 &= \frac{2}{3} (C_3^u - C_3^d), & s_{10} &= \frac{2}{3} (C_4^u - C_4^d).
 \end{aligned} \tag{2.47}$$

The coefficients for the opposite-chirality operators,  $\tilde{s}_{1,\dots,10}$ , are trivially found from the previous ones by replacing  $C_{1,2,3,4}^q \rightarrow \tilde{C}_{1,2,3,4}^q$ . Using the Wilson coefficients  $\vec{s} = (s_1, s_2, \dots, s_{10})^T$  and  $\vec{\tilde{s}} = (\tilde{s}_1, \tilde{s}_2, \dots, \tilde{s}_{10})^T$  at the  $\mu^{\text{SUSY}}$  scale, the dominant box and penguin contributions to  $\varepsilon'_K/\varepsilon_K$  are given by [40]

$$\left. \frac{\varepsilon'_K}{\varepsilon_K} \right|_{\text{box+pen}} = \frac{G_F \omega_+}{2|\varepsilon_K^{\text{EXP}}| \text{Re}A_0^{\text{EXP}}} \langle \vec{Q}_{\varepsilon'}(\mu)^T \rangle \hat{U}(\mu, \mu^{\text{SUSY}}) \text{Im} [\vec{s} - \vec{\tilde{s}}], \tag{2.48}$$

with

$$\omega_+ = (4.53 \pm 0.02) \times 10^{-2}, \tag{2.49}$$

$$|\varepsilon_K^{\text{EXP}}| = (2.228 \pm 0.011) \times 10^{-3}, \tag{2.50}$$

$$\text{Re}A_0^{\text{EXP}} = (3.3201 \pm 0.0018) \times 10^{-7} \text{ GeV}. \tag{2.51}$$

The hadronic matrix elements at  $\mu = 1.3 \text{ GeV}$ , including  $I = 0$  and  $I = 2$  parts, are [40]

$$\langle \vec{Q}_{\varepsilon'}(\mu)^T \rangle = (0.345, 0.133, 0.034, -0.179, 0.152, 0.288, 2.653, 17.305, 0.526, 0.281) (\text{GeV})^3, \tag{2.52}$$

and the approximate function of the RG evolution matrix  $\hat{U}(\mu, \mu^{\text{SUSY}})$  is given in ref. [40].

Next, the  $|\Delta S| = 1$  chromomagnetic-dipole operator that contributes to  $\varepsilon'_K/\varepsilon_K$  is

$$\mathcal{H}_{\text{eff}} = C_g^- Q_g^- + \text{H.c.}, \tag{2.53}$$

with

$$Q_g^- = -\frac{g_s}{(4\pi)^2} (\bar{s} \sigma^{\mu\nu} T^A \gamma_5 d) G_{\mu\nu}^A. \tag{2.54}$$

The complete expression for the Wilson coefficient  $C_g^-$  at the  $\mu^{\text{SUSY}}$  scale is shown in appendix A.3, where  $(\delta_d)_{13}(\delta_d)_{32}$  terms are discarded for simplicity. The corresponding loop functions  $I(x, y)$ ,  $J(x, y)$ ,  $K(x, y)$ ,  $L(x, y)$ ,  $M_3(x)$ , and  $M_4(x)$  are defined in appendix B.2.2.

The chromomagnetic-dipole contribution to  $\varepsilon'_K/\varepsilon_K$  is [43]

$$\frac{\varepsilon'_K}{\varepsilon_K} \Big|_{\text{chromo}} = \frac{\omega_+}{|\varepsilon_K^{\text{EXP}}| \text{Re} A_0^{\text{EXP}}} \left(1 - \hat{\Omega}_{\text{eff}}\right) \frac{11\sqrt{3}}{64\pi^2} \frac{M_\pi^2 M_K^2}{f_\pi(m_s + m_d)} \eta_s B_G \text{Im} C_g^-, \quad (2.55)$$

where  $f_\pi = (130.2 \pm 1.7) \text{ MeV}$  [37], and [58, 67, 68]

$$\hat{\Omega}_{\text{eff}} = 0.148 \pm 0.080, \quad (2.56)$$

$$\eta_s = \left[ \frac{\alpha_s(m_b)}{\alpha_s(1.3 \text{ GeV})} \right]^{\frac{2}{25}} \left[ \frac{\alpha_s(m_t)}{\alpha_s(m_b)} \right]^{\frac{2}{23}} \left[ \frac{\alpha_s(\mu^{\text{SUSY}})}{\alpha_s(m_t)} \right]^{\frac{2}{21}}. \quad (2.57)$$

According to refs. [43, 44], the hadronic matrix element for the chromomagnetic-dipole operator into two pions,  $B_G$ , is enhanced by  $1/N_c \cdot M_K^2/M_\pi^2$  from the large next-to-leading-order corrections that it receives. Therefore, the leading order in the chiral quark model,  $B_G = 1$ , is implausible, and we consider  $B_G = 1 \pm 3$  in our analyses.

The other contributions are negligible [65]. Note that the sub-leading contributions which come from the gluino-mediated photon-penguin and the chargino-mediated  $Z$ -penguins induced by terms of first order in the expansion of the squark mass matrix, have opposite sign and practically cancel each other [65].

Finally, the SUSY contributions to  $\varepsilon'_K/\varepsilon_K$  are given as

$$\left( \frac{\varepsilon'_K}{\varepsilon_K} \right)^{\text{SUSY}} \simeq \frac{\varepsilon'_K}{\varepsilon_K} \Big|_{\text{box+pen}} + \frac{\varepsilon'_K}{\varepsilon_K} \Big|_{\text{chromo}}. \quad (2.58)$$

Note that we discarded the contributions to  $\varepsilon'_K/\varepsilon_K$  from the heavy Higgs exchanges, although they give the strong isospin-violating contribution naturally: the contribution is enhanced by  $\tan^3 \beta$  for only down-type four-fermion scalar operators. These contributions must be proportional to  $m_d m_s$  which cannot be compensated by  $\tan^3 \beta$ , so that they should be the higher-order contributions for  $\varepsilon'_K/\varepsilon_K$ .

## 2.5 $\varepsilon_K$ and $\Delta M_K$

Although  $\varepsilon_K$  is one of the most sensitive quantities to new physics, the SM prediction is still controversial. Especially, the leading short-distance contribution to  $\varepsilon_K$  in the SM is proportional to  $|V_{cb}|^4$  (cf., ref. [69]), whose measured values from inclusive semileptonic  $B$  decays ( $\bar{B} \rightarrow X_c \ell^- \bar{\nu}$ ) and from exclusive decays ( $\bar{B} \rightarrow D^{(*)} \ell^- \bar{\nu}$  and  $\Lambda_b \rightarrow \Lambda_c \ell^- \bar{\nu}$ ) are inconsistent at a  $4.1\sigma$  level [38, 70]. A recent discussion about the exclusive  $|V_{cb}|$  is given in refs. [71–73].

In this paper, for the SM prediction, we use [39]

$$\varepsilon_K^{\text{SM}} = (2.12 \pm 0.18) \times 10^{-3}, \quad (2.59)$$

with

$$\varepsilon_K = e^{i\varphi_\varepsilon} \varepsilon_K^{\text{SM}}, \quad (2.60)$$

where  $\varphi_\varepsilon = \tan^{-1}(2\Delta M_K/\Delta\Gamma_K) = (43.51 \pm 0.05)^\circ$  [37]. This value and the uncertainty are based on the inclusive  $|V_{cb}|$  [38], the Wolfenstein parameters in the angle-only-fit

method [74], and the long-distance contribution obtained by the lattice simulation [32]. Combining the measured value in eq. (2.50), we impose

$$\varepsilon_K^{\text{EXP/SM}} = 1.05 \pm 0.10(\text{TH}), \quad (2.61)$$

on the  $\chi^2$  test, with

$$\varepsilon_K^{\text{SM}} \rightarrow \varepsilon_K^{\text{SM}} + \varepsilon_K^{\text{SUSY}}. \quad (2.62)$$

Note that we also impose  $\text{Re}(\varepsilon_K) > 0$  from  $\text{Re}(\varepsilon_K) = (1.596 \pm 0.013) \times 10^{-3}$  [75].

Within the MSSM, the SUSY contributions to  $\varepsilon_K$  are dominated by gluino box diagrams. In this paper, however, we will focus on their suppressed region. The crossed and uncrossed gluino-box diagrams give opposite sign contributions and there is a certain cancellation region [65, 76], and/or simultaneous mixings of  $(\delta_d^{LL})$  and  $(\delta_d^{RR})$  can also produce the cancellation. Therefore, we also consider the sub-dominant contributions which come from Wino and Higgsino boxes. The  $|\Delta S| = 2$  four-quark effective Hamiltonian at the  $\mu^{\text{SUSY}}$  scale is [77]

$$\mathcal{H}_{\text{eff}} = \sum_{i=1}^5 C_i Q_i + \sum_{i=1}^3 \tilde{C}_i \tilde{Q}_i + \text{H.c.}, \quad (2.63)$$

with

$$\begin{aligned} Q_1 &= (\bar{d}\gamma_\mu P_L s) (\bar{d}\gamma^\mu P_L s), & Q_2 &= (\bar{d}P_L s) (\bar{d}P_L s), & Q_3 &= (\bar{d}_\alpha P_L s_\beta) (\bar{d}_\beta P_L s_\alpha), \\ Q_4 &= (\bar{d}P_L s) (\bar{d}P_R s), & Q_5 &= (\bar{d}_\alpha P_L s_\beta) (\bar{d}_\beta P_R s_\alpha), \\ \tilde{Q}_1 &= (\bar{d}\gamma_\mu P_R s) (\bar{d}\gamma^\mu P_R s), & \tilde{Q}_2 &= (\bar{d}P_R s) (\bar{d}P_R s), & \tilde{Q}_3 &= (\bar{d}_\alpha P_R s_\beta) (\bar{d}_\beta P_R s_\alpha). \end{aligned} \quad (2.64)$$

The kaon mixing amplitude  $M_{12}^{(K)}$ ,  $\Delta M_K$  and  $\varepsilon_K$  are given by

$$M_{12}^{(K)} = \frac{\langle K^0 | \mathcal{H}_{\text{eff}} | \bar{K}^0 \rangle}{2M_K}, \quad (2.65)$$

$$\Delta M_K = 2\text{Re}[M_{12}^{(K)}], \quad (2.66)$$

$$\varepsilon_K = \kappa_\varepsilon \frac{e^{i\varphi_\varepsilon} \text{Im}[M_{12}^{(K)}]}{\sqrt{2} \Delta M_K^{\text{EXP}}} = e^{i\varphi_\varepsilon} \varepsilon_K^{\text{SUSY}}, \quad (2.67)$$

where  $\kappa_\varepsilon = 0.94 \pm 0.02$  [78]. Using the latest lattice result [79], for the hadronic matrix elements, we obtain

$$\langle K^0 | \vec{Q}(\mu) | \bar{K}^0 \rangle = (0.00211, -0.04231, 0.01288, 0.09571, 0.02452) (\text{GeV})^4, \quad (2.68)$$

with  $\langle K^0 | \tilde{Q}_{1,2,3}(\mu) | \bar{K}^0 \rangle = \langle K^0 | Q_{1,2,3}(\mu) | \bar{K}^0 \rangle$ , where  $\mu = 3 \text{ GeV}$  and we used  $m_s(\mu) = (81.64 \pm 1.17) \text{ MeV}$  and  $m_d(\mu) = (2.997 \pm 0.049) \text{ MeV}$  [79].

The leading-order QCD RG corrections are given by [80]

$$C_1(\mu) = \eta_1^K C_1(\mu^{\text{SUSY}}), \quad (2.69)$$

$$\begin{pmatrix} C_2(\mu) \\ C_3(\mu) \end{pmatrix} = X_{23} \eta_{23}^K X_{23}^{-1} \begin{pmatrix} C_2(\mu^{\text{SUSY}}) \\ C_3(\mu^{\text{SUSY}}) \end{pmatrix}, \quad (2.70)$$

$$\begin{pmatrix} C_4(\mu) \\ C_5(\mu) \end{pmatrix} = \begin{pmatrix} (\eta_1^K)^{-4} & \frac{1}{3} \left[ (\eta_1^K)^{-4} - (\eta_1^K)^{\frac{1}{2}} \right] \\ 0 & (\eta_1^K)^{\frac{1}{2}} \end{pmatrix} \begin{pmatrix} C_4(\mu^{\text{SUSY}}) \\ C_5(\mu^{\text{SUSY}}) \end{pmatrix}, \quad (2.71)$$

with

$$\eta_1^K = \left[ \frac{\alpha_s(m_b)}{\alpha_s(\mu)} \right]^{\frac{6}{25}} \left[ \frac{\alpha_s(m_t)}{\alpha_s(m_b)} \right]^{\frac{6}{23}} \left[ \frac{\alpha_s(\mu^{\text{SUSY}})}{\alpha_s(m_t)} \right]^{\frac{6}{21}}, \quad (2.72)$$

$$\eta_{23}^K = \begin{pmatrix} (\eta_1^K)^{\frac{1}{6}(1-\sqrt{241})} & 0 \\ 0 & (\eta_1^K)^{\frac{1}{6}(1+\sqrt{241})} \end{pmatrix}, \quad (2.73)$$

$$X_{23} = \begin{pmatrix} \frac{1}{2}(-15 - \sqrt{241}) & \frac{1}{2}(-15 + \sqrt{241}) \\ 1 & 1 \end{pmatrix}. \quad (2.74)$$

The QCD corrections to  $\tilde{C}_{1,2,3}$  are the same as  $C_{1,2,3}$ .

The Wilson coefficients from the  $|\Delta S| = 2$  gluino boxes are shown in appendix A.4 with their corresponding loop functions defined in appendix B.3.1. In the universal squark mass limit, these results are consistent with ref. [25]. Here, the terms proportional to  $[(\mathcal{M}_D^2)_{LR}]_{12}$  or  $(\delta_d)_{13}(\delta_d)_{32}$  are discarded for simplicity.

The Wilson coefficients and their corresponding loop functions for the sub-leading contributions to  $\varepsilon_K$  are given in appendix A.5 and B.3.2, respectively.

### 3 Parameter scan

The MSSM parameter scan is performed with the framework *Ipanema- $\beta$*  [81] using a GPU of the model GeForce GTX 1080. The samples are a combination of flat scans plus scans based on genetic algorithms [82]. The cost function used by the genetic algorithm is the likelihood function with the observable constrains. In addition, aiming to get a dense population in regions with  $\mathcal{B}(K_S^0 \rightarrow \mu^+ \mu^-)$  significantly different from the SM prediction, specific penalty contributions are added to the total cost function. We also perform specific scans at  $\tan \beta \approx 50$  and  $M_A \approx 1.6$  TeV as for those values the chances to get sizable MSSM effects are larger.

We study three different scenarios (for the ranges of the scanned parameters see table 2):

- Scenario A: a generic scan with universal gaugino masses. No constraint on the Dark Matter relic density is applied in this case, other than the requirement of neutralino Lightest Supersymmetric Particle (LSP). The LSP is Bino-like in most cases, although some points with Higgsino LSP are also found.
- Scenario B: a scan motivated by scenarios with Higgsino Dark Matter. In this scenario, the relic density is mostly function of the LSP mass, which fulfills the measured density [83] at  $m_{\chi_1^0} \approx 1$  TeV [84–87]. Thus, we perform a scan with  $|\mu| = 1$  TeV  $< M_1$ . We assume universal gaugino masses in this scenario, which then implies that  $M_3 > 4.5$  TeV.

Parameter	Scenario A	Scenario B	Scenario C
$\tilde{m}_Q$	[2, 10]	[2, 10]	[4, 10]
$\tilde{m}_Q^2/\tilde{m}_d^2$	[0.25, 4]	[0.25, 4]	[0.25, 4]
$M_3$	[2, 10]	[4.5, 15]	[4, 15]
$\tan \beta$	[10, 50]	[10, 50]	[10, 50]
$M_A$	[1, 2]	[1, 2]	[1, 2]
$ \mu $	[1, 10]	1	[5, 20]
$M_1$	$\frac{\alpha_1(\mu^{\text{SUSY}})}{\alpha_3(\mu^{\text{SUSY}})} M_3$	$\frac{\alpha_1(\mu^{\text{SUSY}})}{\alpha_3(\mu^{\text{SUSY}})} M_3$	5
$M_2$	$\frac{\alpha_2(\mu^{\text{SUSY}})}{\alpha_3(\mu^{\text{SUSY}})} M_3$	$\frac{\alpha_2(\mu^{\text{SUSY}})}{\alpha_3(\mu^{\text{SUSY}})} M_3$	3
$B_G$	[-2, 4]	[-2, 4]	[-2, 4]
Re $\left[ (\delta_d^{LL(RR)})_{12} \right]$	[-0.2, 0.2]	[-0.2, 0.2]	[-0.2, 0.2]
Im $\left[ (\delta_d^{LL(RR)})_{12} \right]$	[-0.2, 0.2]	[-0.2, 0.2]	[-0.2, 0.2]

**Table 2.** Scan ranges for scenario A, B (motivated by Higgsino Dark Matter) and C (motivated by Wino Dark Matter). All masses are in TeV. The nuisance parameter  $B_G$  appears in the chromomagnetic-dipole contribution to  $\epsilon'_K/\epsilon_K$ .

- Scenario C: a scan motivated by scenarios with Wino Dark Matter, which is possible in mAMSB or pMSSM, although it is under pressure by  $\gamma$ -rays and antiprotons data [88]. In those scenarios, the relic density is mostly function of the LSP mass, which fulfills the experimental value [83] at  $m_{\chi_1^0} \approx 3$  TeV [87, 89]. Thus, we make a scan with  $M_2 = 3$  TeV  $< |\mu|, M_{1,3}$ . The Bino mass  $M_1$  is set to 5 TeV for simplicity. Since it is only necessary in order to ensure that the LSP is Wino-like, any other value above 3 TeV (such as, e.g., an mAMSB-like relation  $M_1 \approx 9.7$  TeV) could also be used without changing the obtained results. The lightest neutralino and the lightest chargino are nearly degenerate, and radiative corrections are expected to bring the chargino mass to be  $\approx 160$  MeV heavier than the lightest neutralino [90].

For simplicity, in all cases we set to zero the trilinear couplings and the mass insertions other than  $(\delta_d^{LL(RR)})_{12}$  and  $(\delta_u^{LL})_{12}$  which is given by the relations in eq. (2.2), and  $\mu$  is treated as a real parameter, with both signs allowed a priori.

We also perform studies at the MFV limit, using RG equations induced MIs in CMSSM. As expected, no significant effect is found in this case.

For the squark masses, we use  $\tilde{m}_Q = \tilde{m}_u \neq \tilde{m}_d$ . This set up is motivated by the SUSY SU(5) grand unified theory, where  $Q$  and  $U$ -squark are contained in  $\mathbf{10}$  representation matter multiplet while  $D$ -squark is in  $\bar{\mathbf{5}}$  representation one. In general, their soft-SUSY breaking masses are different and depend on couplings between the matter multiplets and the SUSY breaking spurion field.

## 4 Results

In the following, we show the main results of our scans. The points with  $\chi^2 < 12.5$ , corresponding to 95% C.L. for six degrees of freedom, are considered experimentally viable.



The number of degrees of freedom has been calculated as the number of observables, not counting the nuisance parameter  $B_G$ , the rigid bound on the  $\tan\beta:M_A$  plane, and  $\Delta M_K$ , which are not Gaussian distributed. Therefore, the  $\chi^2$  requirement corresponds to a 95% C.L. or tighter. Similar plots are obtained if one uses a looser bound on the absolute  $\chi^2$  accompanied with a  $\Delta\chi^2 < 5.99$  across the plane being plotted. Due to the large theory uncertainty,  $\mathcal{B}(K_L^0 \rightarrow \mu^+\mu^-)$  can go up to  $\approx 1 \times 10^{-8}$  at  $2\sigma$  level. Values slightly above that limit can still be allowed if they reduce the  $\chi^2$  contribution in other observables. The allowed regions are separated by the sign of  $A_{L\gamma\gamma}^\mu$  in eq. (2.16). We also show results for  $A_{CP}$ , which could be experimentally accessed by means of a tagged analysis.

#### 4.1 Effects from $\left(\delta_d^{LL(RR)}\right)_{12}$ separately

We first study separately the effects of pure left-handed or pure right-handed MIs, to study the regions of the MSSM parameter space in which either  $LL$  MIs or  $RR$  MIs dominate.<sup>7</sup> The obtained scatter plots for  $\mathcal{B}(K_L^0 \rightarrow \mu^+\mu^-)$  vs.  $\mathcal{B}(K_S^0 \rightarrow \mu^+\mu^-)$  and  $\mathcal{B}(K_S^0 \rightarrow \mu^+\mu^-)$  vs.  $\varepsilon'_K/\varepsilon_K$  are shown in figure 2 and figure 3 for Scenario A, figure 4 and figure 5 for Scenario B, and figure 6 and figure 7 for Scenario C. The points in the planes correspond to predictions from different values of the input parameters. One should note that in such cases, the SUSY contributions to  $\varepsilon_K$  can be suppressed naturally in a heavy gluino region ( $M_3 \gtrsim 1.5\tilde{m}_Q$ ) [65, 76].

In Scenario A (see figure 2) and Scenario C (see figure 6), we can see that the 95% C.L. allowed regions for  $\mathcal{B}(K_S^0 \rightarrow \mu^+\mu^-)$  in light of the constraints listed in table 1 are approximately  $[0.78, 14] \times 10^{-12}$  for  $LL$ -only contributions, and  $[1.5, 35] \times 10^{-12}$  for  $RR$ -only contributions, without any need of fine-tuning the parameters to avoid constraints from  $\mathcal{B}(K_L^0 \rightarrow \mu^+\mu^-)$ . The MSSM contributions are similar for  $RR$  and  $LL$ , and the differences on the allowed ranges for  $\mathcal{B}(K_S^0 \rightarrow \mu^+\mu^-)$  arise from the interference with the SM amplitudes in  $K_{S(L)}^0 \rightarrow \mu^+\mu^-$ , which are shown in section 2.3. The allowed regions for scenarios A and C are very similar to each other, although marginally larger on A. It can also be seen that, in Scenario B (see figure 4) the maximum departure of  $\mathcal{B}(K_S^0 \rightarrow \mu^+\mu^-)$  from the SM is smaller than in the other scenarios, since  $C_{S,P} \propto \mu$  and  $\mu$  is small relative to squark and gluino masses. In the contributions to  $(\varepsilon'_K/\varepsilon_K)^{\text{SUSY}}$ , the chromomagnetic-dipole contribution can be significant in both  $LL$ -only and  $RR$ -only cases when  $\mu \tan\beta$  and  $B_G$  have large values, while the box contributions can be significant only via  $LL$  MIs [65]. Note that the penguin contributions to  $(\varepsilon'_K/\varepsilon_K)^{\text{SUSY}}$  are neglected in our parameter scan.

The effective branching fraction and  $CP$  asymmetry are shown in figure 8 for Scenario A. Note that the negative value of  $\mathcal{B}(K_S^0 \rightarrow \mu^+\mu^-)_{\text{eff}}$  is compensated in data by inclusion of the background events from  $K_L^0 \rightarrow \mu^+\mu^-$ , so that the overall  $K^0 \rightarrow \mu^+\mu^-$  is always positive. Correlation patterns of  $A_{CP}$  with other observables can be seen in figure 9, where we choose  $D' = -D$  and  $D = 0.5$  for simplicity. We find that  $CP$  asymmetries can be up to  $\approx 6$  (at  $D = 1$ ), approximately eight times bigger than in the SM. The largest effects are found in left-handed scenarios.

<sup>7</sup>As an example, MFV models the  $LL$  MIs can become non-zero after RGE, which does not happen for  $RR$  MIs.

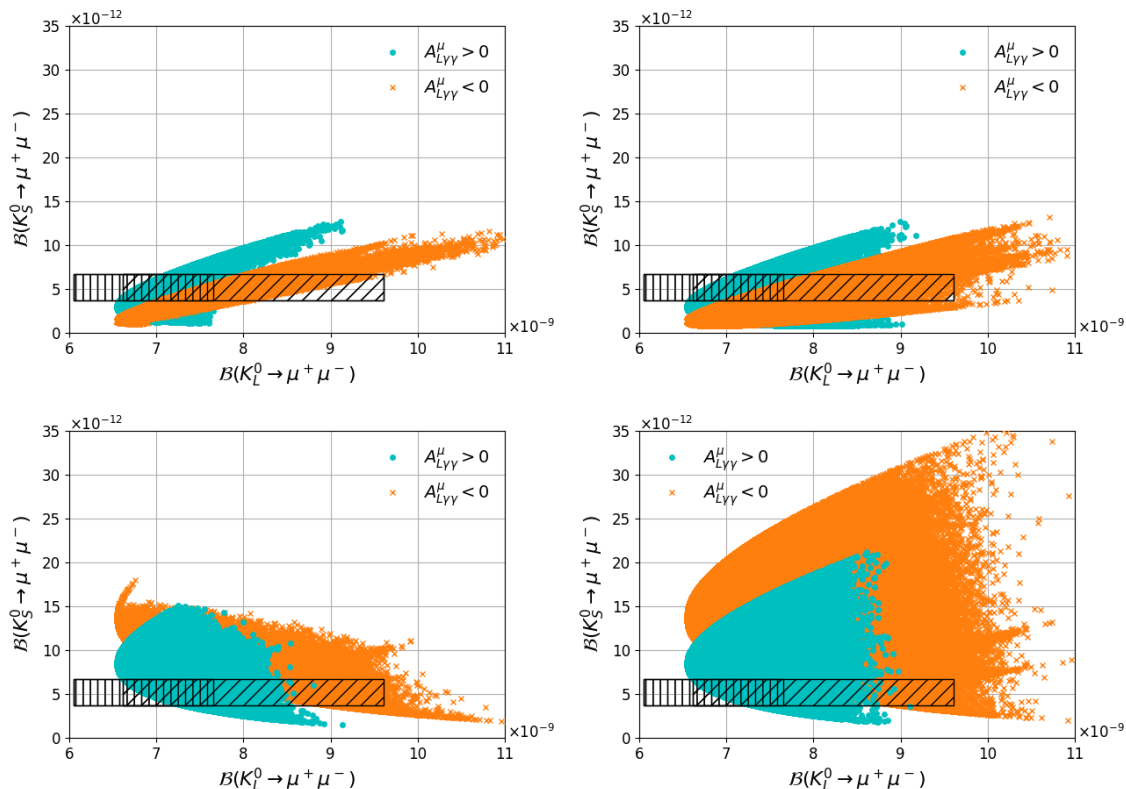


**Figure 2.** Scenario A  $\mathcal{B}(K_S^0 \rightarrow \mu^+ \mu^-)$  vs.  $\mathcal{B}(K_L^0 \rightarrow \mu^+ \mu^-)$  for  $(\delta_d^{LL})_{12} \neq 0$  and  $(M_3 \cdot \mu) > 0$  (upper left),  $(\delta_d^{LL})_{12} \neq 0$  and  $(M_3 \cdot \mu) < 0$  (upper right),  $(\delta_d^{RR})_{12} \neq 0$  and  $(M_3 \cdot \mu) > 0$  (lower left), and  $(\delta_d^{RR})_{12} \neq 0$  and  $(M_3 \cdot \mu) < 0$  (lower right). The cyan dots correspond to  $A_{L\gamma\gamma}^\mu > 0$  and the orange crosses to  $A_{L\gamma\gamma}^\mu < 0$ . The vertically hatched area corresponds to the SM prediction for  $A_{L\gamma\gamma}^\mu > 0$  and the inclined hatched area corresponds to the SM prediction for  $A_{L\gamma\gamma}^\mu < 0$ .

## 4.2 Floating $LL$ and $RR$ MIs simultaneously

A priori, one possibility to avoid the constraint from  $\mathcal{B}(K_L^0 \rightarrow \mu^+ \mu^-)$  is to allow simultaneously for non-zero  $LL$  and  $RR$  mass insertions. This way both  $C_{S(P)}$  and  $\tilde{C}_{S(P)}$  are non zero and eqs. (2.19)–(2.24) do not hold. One can then find regions in which the MSSM contributions to  $\mathcal{B}(K_S^0 \rightarrow \mu^+ \mu^-)$  do not alter  $\mathcal{B}(K_L^0 \rightarrow \mu^+ \mu^-)$  significantly.

For instance, if one chooses

$$\text{Re}[(\delta_d^{LL})_{12}] = -\text{Re}[(\delta_d^{RR})_{12}], \quad \text{Im}[(\delta_d^{LL})_{12}] = \text{Im}[(\delta_d^{RR})_{12}], \quad (4.1)$$

then the SUSY contributions to  $\mathcal{B}(K_L^0 \rightarrow \mu^+ \mu^-)$  are canceled, while the SUSY contributions to  $\mathcal{B}(K_S^0 \rightarrow \mu^+ \mu^-)$  are maximized (see eqs. (2.9)–(2.13)). However, it is known that in those cases the bounds from  $\Delta M_K$  and  $\varepsilon_K$  are very stringent. Using genetic algorithms with cost functions that target large values of  $\mathcal{B}(K_S^0 \rightarrow \mu^+ \mu^-)$ , we find fine-tuned regions with  $\mathcal{B}(K_S^0 \rightarrow \mu^+ \mu^-) > 10^{-10}$ , or even at the level of the current experimental bound of  $8 \times 10^{-10}$  at 90% C.L. [22], which are consistent with all our constraints. These points are located along very narrow strips in the  $(\delta_d^{LL})_{12}$  vs.  $(\delta_d^{RR})_{12}$  planes, as shown in figure 10. The figure corresponds to Scenario C as it is the one with higher density of

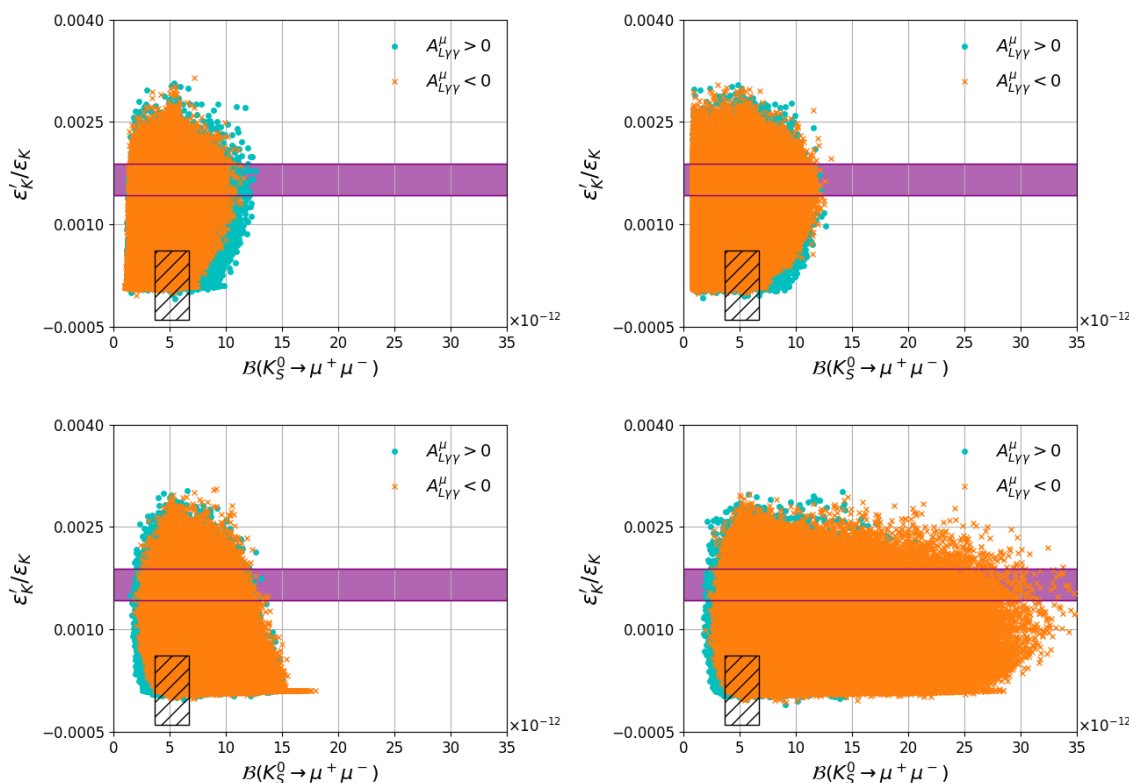


**Figure 3.** Scenario A  $\frac{\varepsilon'_K}{\varepsilon_K}$  vs.  $\mathcal{B}(K_S^0 \rightarrow \mu^+ \mu^-)$  for  $(\delta_d^{LL})_{12} \neq 0$  and  $(M_3 \cdot \mu) > 0$  (upper left),  $(\delta_d^{LL})_{12} \neq 0$  and  $(M_3 \cdot \mu) < 0$  (upper right),  $(\delta_d^{RR})_{12} \neq 0$  and  $(M_3 \cdot \mu) > 0$  (lower left), and  $(\delta_d^{RR})_{12} \neq 0$  and  $(M_3 \cdot \mu) < 0$  (lower right). The cyan dots correspond to  $A_{L\gamma\gamma}^\mu > 0$  and the orange crosses to  $A_{L\gamma\gamma}^\mu < 0$ . The deep purple band corresponds to the experimental results and the hatched area to the SM prediction.

points at large values of  $\mathcal{B}(K_S^0 \rightarrow \mu^+ \mu^-)$  and the pattern observed in Scenario A is nearly identical. A particularly favorable region corresponds to  $|(\delta_d^{LL})_{12}| \approx 2|(\delta_d^{RR})_{12}| \sim 0.03$  and  $\arg [(\delta_d^{LL})_{12}] \approx -\arg [(\delta_d^{RR})_{12}] + \pi$ , which is in the vicinity of eq. (4.1), and with  $\delta_u^{LL}$  given by the symmetry relation of eq. (2.2). They also favor narrow regions in the squark vs. gluino masses planes as shown in figure 11. We checked that the values close to the experimental upper bound can still be obtained even if the constraint on  $\Delta M_K$  is significantly tightened.

We note that the authors in ref. [38] provide a SM prediction for  $\varepsilon_K$  less consistent with data than the one we used. That prediction is obtained using  $|V_{cb}|$  from exclusive decays. If we use that value instead of eq. (2.61),

$$\varepsilon_K^{\text{EXP/SM}} = 1.41 \pm 0.16(\text{TH}), \tag{4.2}$$

then we can accommodate more easily  $LL$  and  $RR$  MIs of similar sizes, and fine-tuned regions with  $\mathcal{B}(K_S^0 \rightarrow \mu^+ \mu^-) > 10^{-10}$  are found with higher chances. The shapes of the strips in the mass insertion planes do not change substantially.

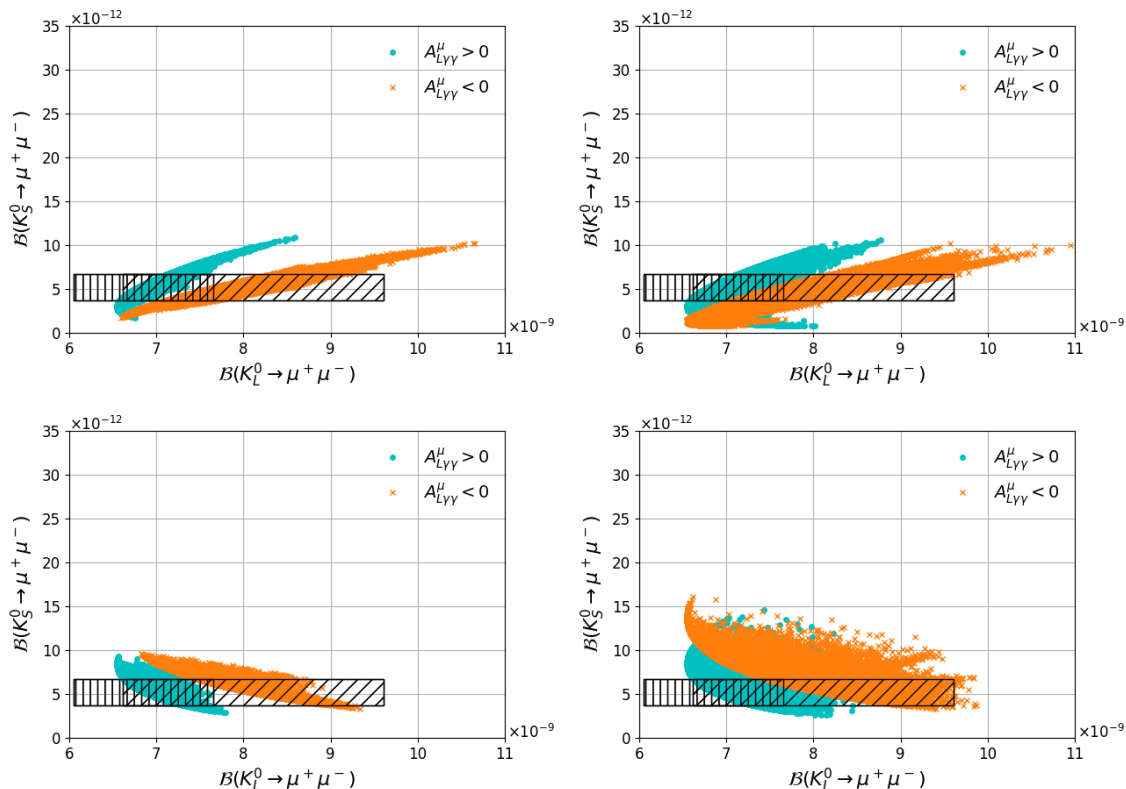


**Figure 4.** Scenario B, motivated by Higgsino Dark Matter with universal gaugino masses,  $\mathcal{B}(K_S^0 \rightarrow \mu^+ \mu^-)$  vs.  $\mathcal{B}(K_L^0 \rightarrow \mu^+ \mu^-)$  for  $(\delta_d^{LL})_{12} \neq 0$  and  $(M_3 \cdot \mu) > 0$  (upper left),  $(\delta_d^{LL})_{12} \neq 0$  and  $(M_3 \cdot \mu) < 0$  (upper right),  $(\delta_d^{RR})_{12} \neq 0$  and  $(M_3 \cdot \mu) > 0$  (lower left), and  $(\delta_d^{RR})_{12} \neq 0$  and  $(M_3 \cdot \mu) < 0$  (lower right). The cyan dots correspond to  $A_{L\gamma\gamma}^\mu > 0$  and the orange crosses to  $A_{L\gamma\gamma}^\mu < 0$ . The vertically hatched area corresponds to the SM prediction for  $A_{L\gamma\gamma}^\mu > 0$  and the inclined hatched area corresponds to the SM prediction for  $A_{L\gamma\gamma}^\mu < 0$ .

### 4.3 Non degenerate Higgs masses

The results so far have been obtained in the MSSM framework, in which  $|C_S| \approx |C_P|$ . This is due to the mass degeneracy  $M_H \approx M_A$ . In models in which such degeneracy can be broken, the constraint that  $\mathcal{B}(K_L^0 \rightarrow \mu^+ \mu^-)$  imposes to  $\mathcal{B}(K_S^0 \rightarrow \mu^+ \mu^-)$  relaxes the more those two masses differ. This degeneracy is broken in MSSM at low values of  $M_A$ , and requiring  $\tan\beta$  to be small to avoid constraints from  $\tan\beta : M_A$  planes from LHC. Those regions are more difficult to study, since it would require a detailed specification of the MSSM and test it against bounds of the Higgs sector. The mass degeneracy is also broken in extensions such as NMSSM. According to our scans, on those cases one could, in principle, reach values of  $\mathcal{B}(K_S^0 \rightarrow \mu^+ \mu^-) > 10^{-10}$  for mass differences of  $\mathcal{O}(33\%)$  or larger without fine-tuning the MIs.

## 5 Conclusions

We explored MSSM contribution to  $\mathcal{B}(K_S^0 \rightarrow \mu^+ \mu^-)$  for non-zero  $(\delta_d^{LL})_{12}$  and  $(\delta_d^{RR})_{12}$  mass insertions, motivated by the experimental value of  $\varepsilon'_K/\varepsilon_K$ , and in the large  $\tan\beta$  regime. The expressions for the relevant MSSM amplitudes have been provided. We find

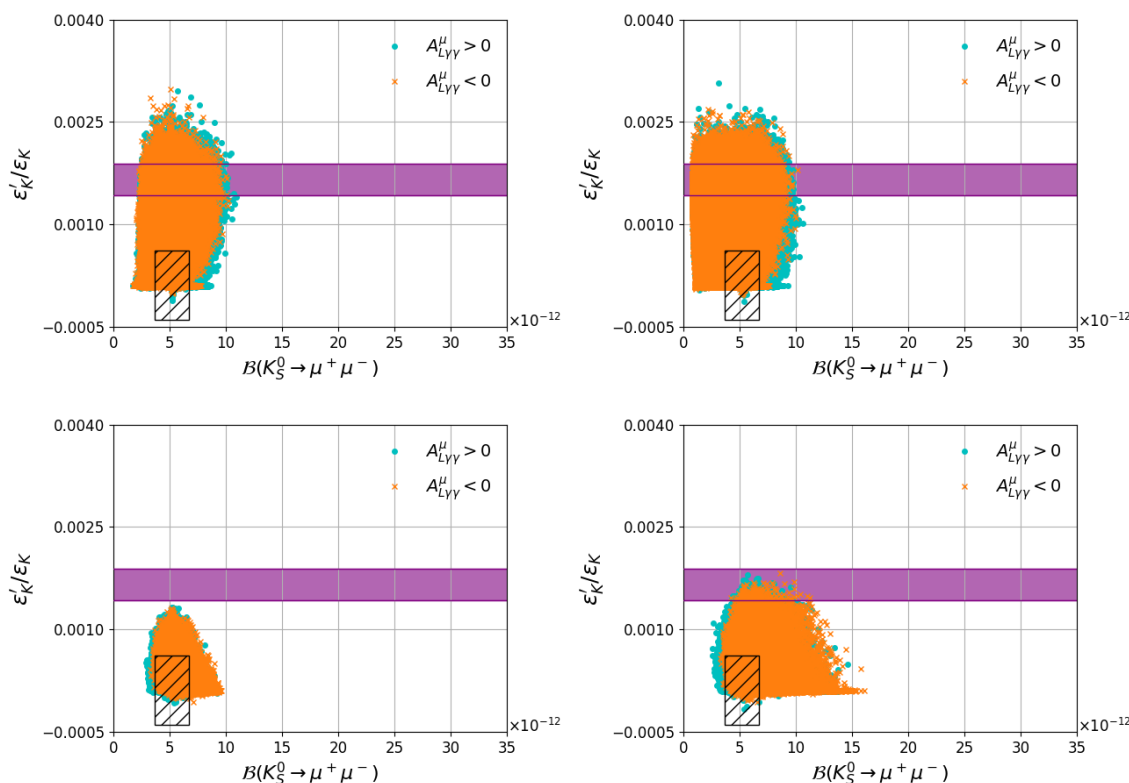


**Figure 5.** Scenario B, motivated by Higgsino Dark Matter and universal gaugino masses,  $\frac{\epsilon'_K}{\epsilon_K}$  vs.  $\mathcal{B}(K_S^0 \rightarrow \mu^+\mu^-)$  for  $(\delta_d^{LL})_{12} \neq 0$  and  $(M_3 \cdot \mu) > 0$  (upper left),  $(\delta_d^{LL})_{12} \neq 0$  and  $(M_3 \cdot \mu) < 0$  (upper right),  $(\delta_d^{RR})_{12} \neq 0$  and  $(M_3 \cdot \mu) > 0$  (lower left), and  $(\delta_d^{RR})_{12} \neq 0$  and  $(M_3 \cdot \mu) < 0$  (lower right). The cyan dots correspond to  $A_{L\gamma\gamma}^\mu < 0$  and the orange crosses to  $A_{L\gamma\gamma}^\mu > 0$ . The deep purple band corresponds to the experimental results and the hatched area to the SM prediction.

that MSSM contributions to  $\mathcal{B}(K_S^0 \rightarrow \mu^+\mu^-)$  can surpass the SM contributions [ $\mathcal{B}(K_S^0 \rightarrow \mu^+\mu^-)^{\text{SM}} = 5.18 \times 10^{-12}$ ] by up to a factor of seven (see figure 2), reaching the level of  $3.5 \times 10^{-11}$  even for large SUSY masses, with no conflict with existing experimental data, and are detectable by LHCb. This is also the case even if  $\epsilon'_K/\epsilon_K$  turns out to be SM-like as predicted by refs. [33–35]. Figures of correlations between  $\mathcal{B}(K_S^0 \rightarrow \mu^+\mu^-)$  and other observables have been provided for different regions of the MSSM parameter space, and can be used to understand which scenarios are more or less favoured, depending on the experimental outcomes. The  $3.5 \times 10^{-11}$  bound is due to the combined effect of  $\Delta M_K, \epsilon_K$ , and  $K_L^0 \rightarrow \mu^+\mu^-$  constraints. Such bound is not rigid, and fine-tuned regions can bring the branching fraction above the  $10^{-10}$  level, even up to the current experimental bound; the largest deviations from SM are found at  $|(\delta_d^{LL})_{12}| \approx 2|(\delta_d^{RR})_{12}| \sim 0.03$  and  $\arg [(\delta_d^{LL})_{12}] \approx -\arg [(\delta_d^{RR})_{12}] + \pi$  for large squark and gluino masses. We also find that the  $CP$  asymmetry of  $K^0 \rightarrow \mu^+\mu^-$  can be significantly modified by MSSM contributions, being up to eight times bigger than the SM prediction in the pure LL case. Finally, we remind that, for simplicity, we have restricted our study to the main contributions in the large  $\tan\beta$  regime. Discarded terms could, in principle, provide even more flexibility to the allowed regions.

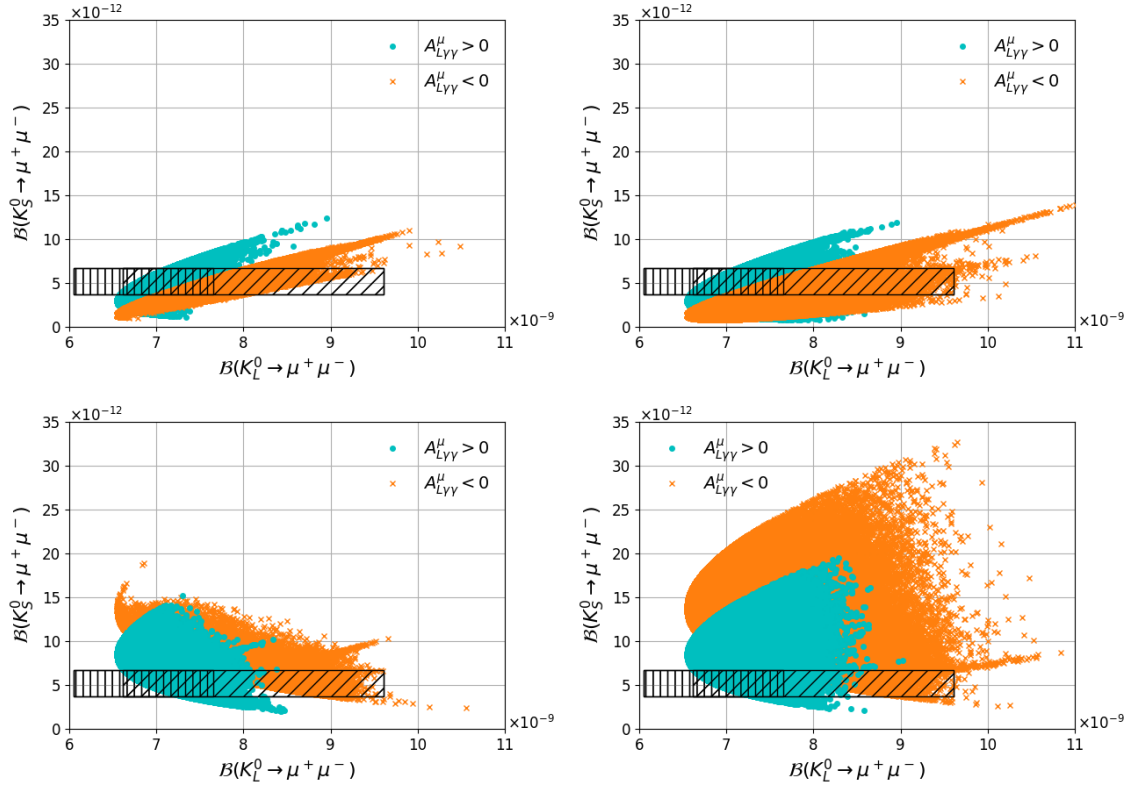


**Figure 6.** Scenario C (motivated by Wino Dark Matter)  $\mathcal{B}(K_S^0 \rightarrow \mu^+ \mu^-)$  vs.  $\mathcal{B}(K_L^0 \rightarrow \mu^+ \mu^-)$  for  $(\delta_d^{LL})_{12} \neq 0$  and  $(M_3 \cdot \mu) > 0$  (upper left),  $(\delta_d^{LL})_{12} \neq 0$  and  $(M_3 \cdot \mu) < 0$  (upper right),  $(\delta_d^{RR})_{12} \neq 0$  and  $(M_3 \cdot \mu) > 0$  (lower left), and  $(\delta_d^{RR})_{12} \neq 0$  and  $(M_3 \cdot \mu) < 0$  (lower right). The cyan dots correspond to  $A_{L\gamma\gamma}^\mu > 0$  and the orange crosses to  $A_{L\gamma\gamma}^\mu < 0$ . The vertically hatched area corresponds to the SM prediction for  $A_{L\gamma\gamma}^\mu > 0$  and the inclined hatched area corresponds to the SM prediction for  $A_{L\gamma\gamma}^\mu < 0$ .

## Acknowledgments

We would like to thank A. Crivellin, G. Isidori, T. Kuwahara, D. Mueller, and K.A. Olive for useful discussions. The research activity of IGFAE/USC members is partially funded by ERC-StG-639068 and partially by XuntaGal. G. D. was supported in part by MIUR under Project No. 2015P5SBHT (PRIN 2015) and by the INFN research initiative ENP. K. Y. was supported by Grant-in-Aid for Scientific research from the Ministry of Education, Science, Sports, and Culture (MEXT), Japan, No. 16H06492.

## A Wilson coefficients

### A.1 $|\Delta S| = 1$ gluino box contribution

The Wilson coefficients of the gluino box contributions to  $\varepsilon'_K/\varepsilon_K$  are

$$C_1^q = \frac{(\alpha_s)^2}{2\sqrt{2}G_F M_3^2} (\delta_d^{LL})_{12} \left[ \frac{1}{18} f(x_3^Q, x_3^q) - \frac{5}{18} g(x_3^Q, x_3^q) \right],$$

$$C_2^q = \frac{(\alpha_s)^2}{2\sqrt{2}G_F M_3^2} (\delta_d^{LL})_{12} \left[ \frac{7}{6} f(x_3^Q, x_3^q) + \frac{1}{6} g(x_3^Q, x_3^q) \right],$$

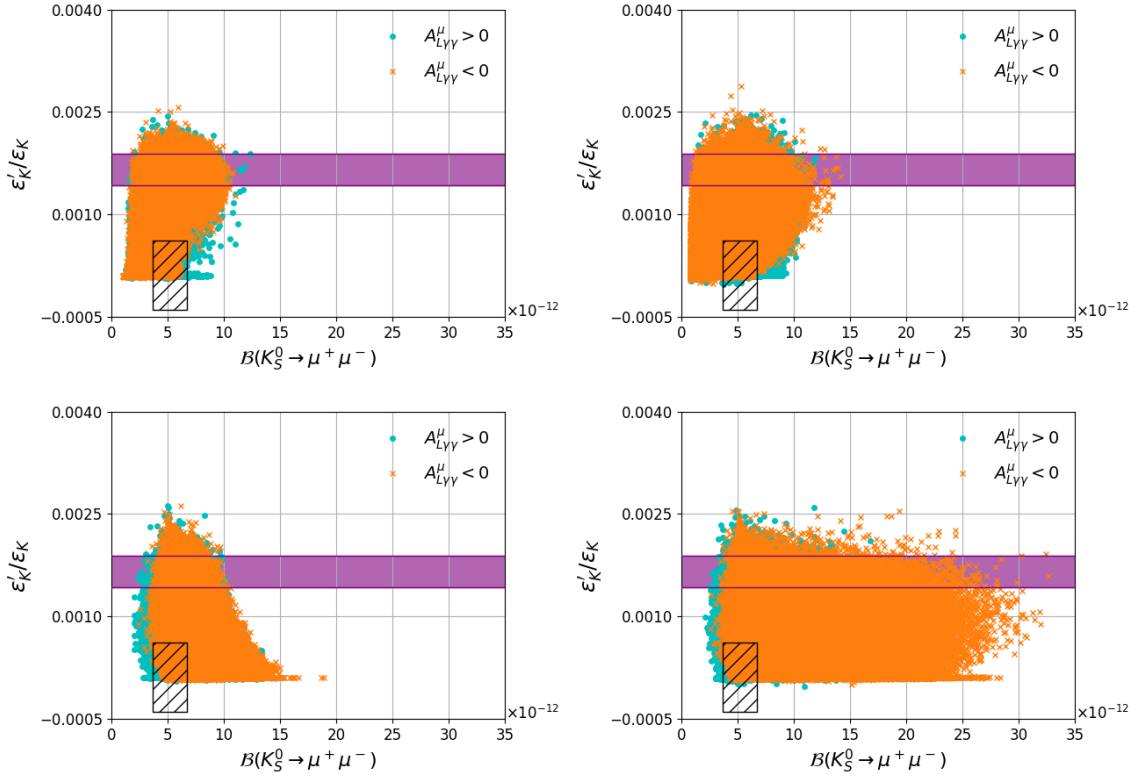


**Figure 7.** Scenario C, motivated by Wino Dark Matter,  $\frac{\epsilon'_K}{\epsilon_K}$  vs.  $\mathcal{B}(K_S^0 \rightarrow \mu^+ \mu^-)$  for  $(\delta_d^{LL})_{12} \neq 0$  and  $(M_3 \cdot \mu) > 0$  (upper left),  $(\delta_d^{LL})_{12} \neq 0$  and  $(M_3 \cdot \mu) < 0$  (upper right),  $(\delta_d^{RR})_{12} \neq 0$  and  $(M_3 \cdot \mu) > 0$  (lower left), and  $(\delta_d^{RR})_{12} \neq 0$  and  $(M_3 \cdot \mu) < 0$  (lower right). The cyan dots correspond to  $A_{L\gamma\gamma}^\mu > 0$  and the orange crosses to  $A_{L\gamma\gamma}^\mu < 0$ . The deep purple band corresponds to the experimental results and the hatched area to the SM prediction.

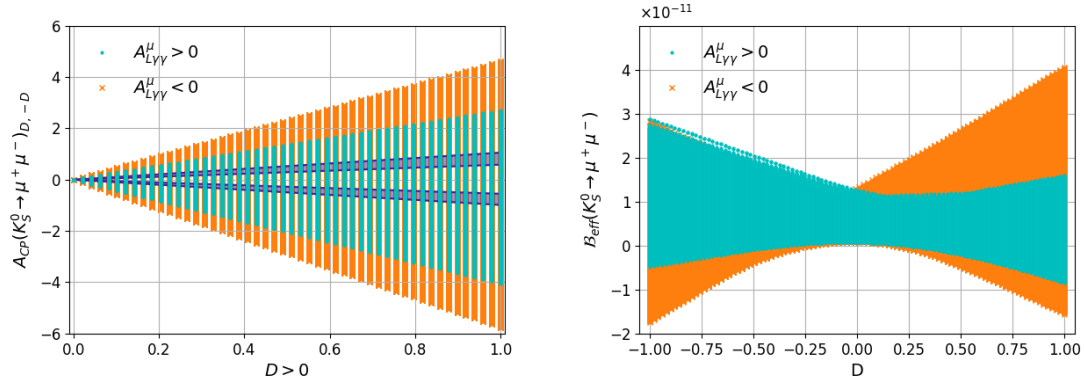


**Figure 8.** Scenario A,  $(\delta_d^{LL})_{12} \neq 0$  and  $(M_3 \cdot \mu) < 0$ . Plots of  $A_{CP}(K_S^0 \rightarrow \mu^+ \mu^-)_{D, -D}$  vs.  $D$  (left) for the case  $D = -D'$  ( $D > 0$ ) where the cyan dots correspond to  $A_{L\gamma\gamma}^\mu > 0$ , the orange crosses to  $A_{L\gamma\gamma}^\mu < 0$ , and the deep purple bands correspond to the SM predictions in eq. (2.33).  $\mathcal{B}(K_S^0 \rightarrow \mu^+ \mu^-)_{\text{eff}}$  vs.  $D$  (right).

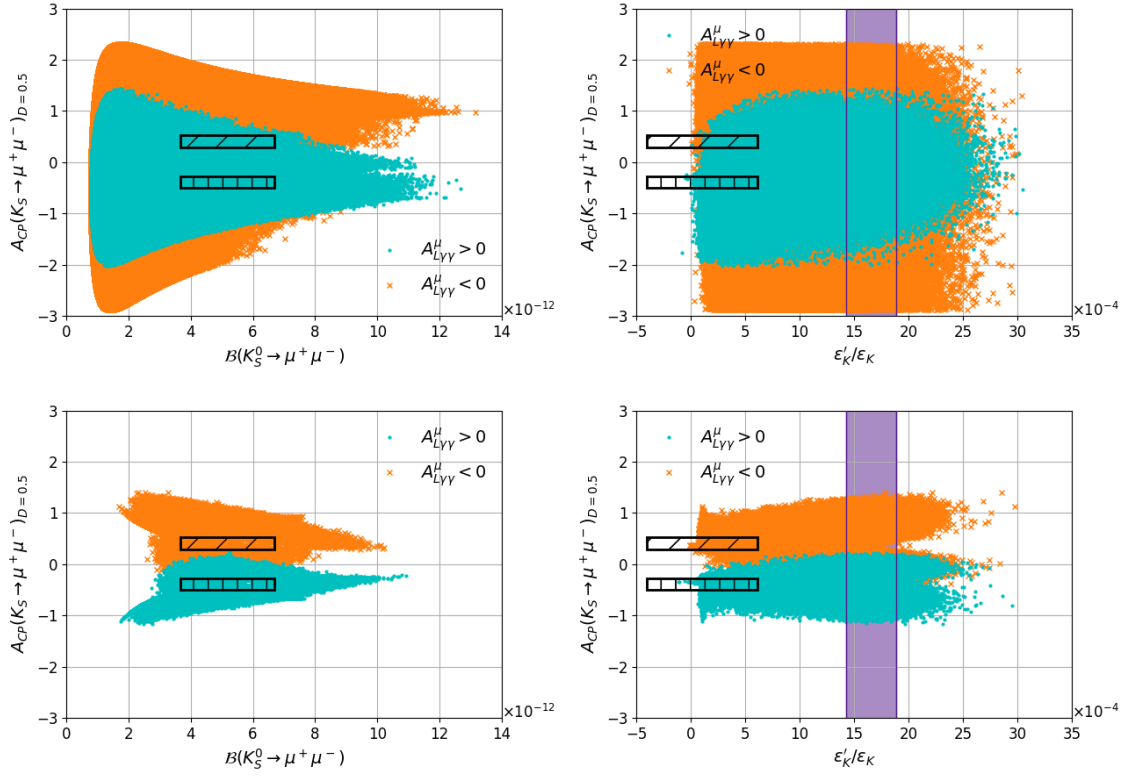


**Figure 9.**  $A_{CP}$  vs.  $\mathcal{B}(K_S^0 \rightarrow \mu^+ \mu^-)$  (left) and vs.  $\epsilon'_K/\epsilon_K$  (right). The top panels correspond to Scenario A,  $(\delta_d^{LL})_{12} \neq 0$  and  $(M_3 \cdot \mu) < 0$ . The bottom panels correspond to Scenario B,  $(\delta_d^{LL})_{12} \neq 0$  and  $(M_3 \cdot \mu) > 0$ . The plots are done for  $D = -D' = 0.5$ . The cyan dots correspond to  $A_{L\gamma\gamma}^\mu > 0$  and the orange crosses to  $A_{L\gamma\gamma}^\mu < 0$ . The deep purple bands correspond to the experimental value of  $\epsilon'_K/\epsilon_K$ , the vertically hatched areas correspond to the SM prediction for  $A_{L\gamma\gamma}^\mu > 0$  and the inclined hatched areas to the SM prediction for  $A_{L\gamma\gamma}^\mu < 0$ .

$$\begin{aligned}
 C_3^q &= \frac{(\alpha_s)^2}{2\sqrt{2}G_F M_3^2} (\delta_d^{LL})_{12} \left[ -\frac{5}{9} f(x_3^Q, x_3^Q) + \frac{1}{36} g(x_3^Q, x_3^Q) \right], \\
 C_4^q &= \frac{(\alpha_s)^2}{2\sqrt{2}G_F M_3^2} (\delta_d^{LL})_{12} \left[ \frac{1}{3} f(x_3^Q, x_3^Q) + \frac{7}{12} g(x_3^Q, x_3^Q) \right], \\
 \tilde{C}_1^q &= \frac{(\alpha_s)^2}{2\sqrt{2}G_F M_3^2} (\delta_d^{RR})_{12} \left[ \frac{1}{18} f(x_3^d, x_3^Q) - \frac{5}{18} g(x_3^d, x_3^Q) \right], \\
 \tilde{C}_2^q &= \frac{(\alpha_s)^2}{2\sqrt{2}G_F M_3^2} (\delta_d^{RR})_{12} \left[ \frac{7}{6} f(x_3^d, x_3^Q) + \frac{1}{6} g(x_3^d, x_3^Q) \right], \\
 \tilde{C}_3^q &= \frac{(\alpha_s)^2}{2\sqrt{2}G_F M_3^2} (\delta_d^{RR})_{12} \left[ -\frac{5}{9} f(x_3^d, x_3^q) + \frac{1}{36} g(x_3^d, x_3^q) \right], \\
 \tilde{C}_4^q &= \frac{(\alpha_s)^2}{2\sqrt{2}G_F M_3^2} (\delta_d^{RR})_{12} \left[ \frac{1}{3} f(x_3^d, x_3^q) + \frac{7}{12} g(x_3^d, x_3^q) \right], \tag{A.1}
 \end{aligned}$$

where  $q$  runs  $u$  and  $d$ , and  $x_3^Q = \tilde{m}_Q^2/M_3^2$  and  $x_3^q = \tilde{m}_q^2/M_3^2$ .



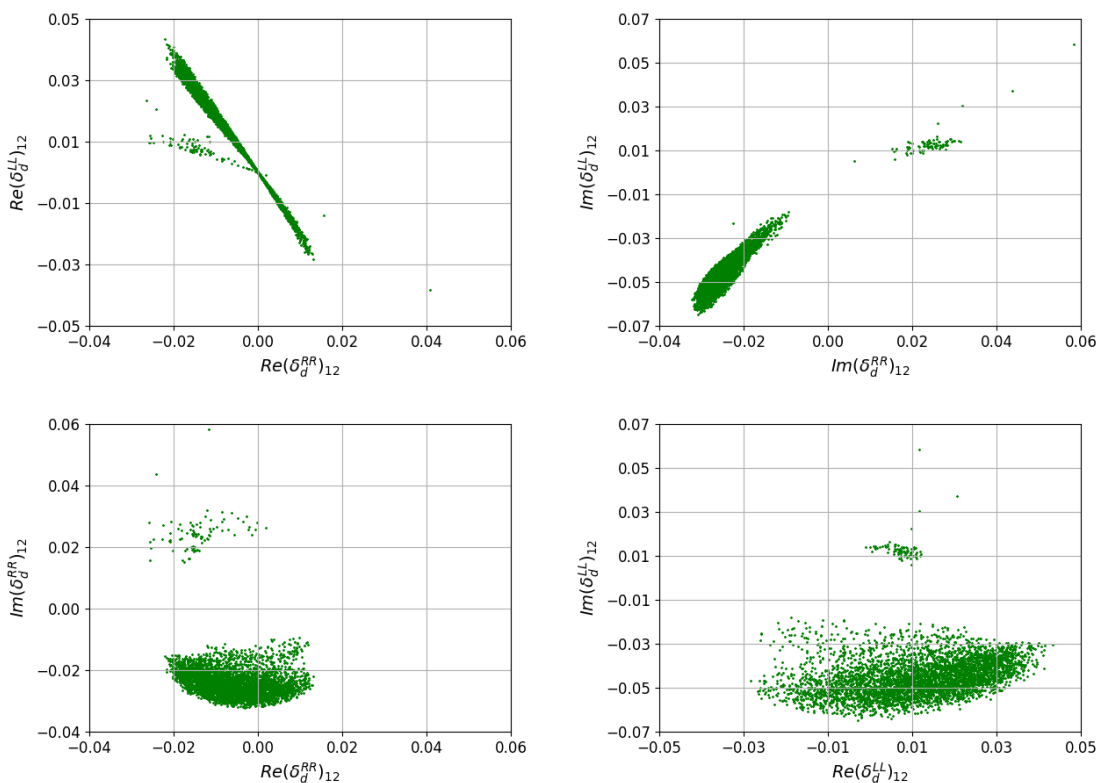


**Figure 10.** Scatter plots of the real (upper left) and the imaginary (upper right) parts of the mass insertions  $(\delta_d^{RR})_{12}$  and  $(\delta_d^{LL})_{12}$  for  $\mathcal{B}(K_S^0 \rightarrow \mu^+ \mu^-) > 2 \times 10^{-10}$ , of the real vs. imaginary  $(\delta_d^{RR})_{12}$  (lower left) and of the real vs. imaginary  $(\delta_d^{LL})_{12}$  (lower right). All points in the plane pass the experimental constraints defined in section 2. The up-type MI  $(\delta_u^{LL})_{12}$  is given by eq. (2.2). The plots correspond to Scenario C, with a sample of 4378 points with  $\mathcal{B}(K_S^0 \rightarrow \mu^+ \mu^-) > 2 \times 10^{-10}$  and  $\chi^2 < 12.5$ , produced after 6M generations of 200k points each. The pattern observed in Scenario A is very similar.

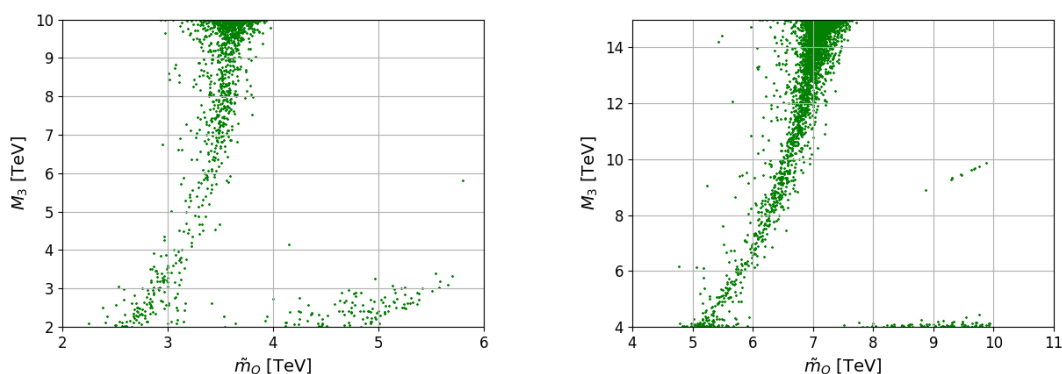


**Figure 11.** Scatter plot of the squark and gluino masses for  $\mathcal{B}(K_S^0 \rightarrow \mu^+ \mu^-) > 2 \times 10^{-10}$  taking into account the constraints defined in section 2. Left: scenario A, Right: scenario C. The  $\chi^2$  cut in Scenario A has been relaxed to 14 to increase the density of points.

## A.2 $|\Delta S| = 1$ chargino-mediated Z-penguin contribution

The Wilson coefficients of the chargino-mediated Z-penguin are

$$\begin{aligned}
 C_1^u &= -\frac{(\alpha_2)^2 \sin^2 \theta_W}{12\sqrt{2}G_F M_W^2} \frac{[(\mathcal{M}_U^2)_{LR}]_{23}^* [(\mathcal{M}_U^2)_{LR}]_{13}}{M_2^4} l(x_2^Q, x_2^u), \\
 C_1^d &= \frac{(\alpha_2)^2 \sin^2 \theta_W}{24\sqrt{2}G_F M_W^2} \frac{[(\mathcal{M}_U^2)_{LR}]_{23}^* [(\mathcal{M}_U^2)_{LR}]_{13}}{M_2^4} l(x_2^Q, x_2^u), \\
 C_3^u &= \frac{(\alpha_2)^2}{16\sqrt{2}G_F M_W^2} \left(1 - \frac{4}{3} \sin^2 \theta_W\right) \frac{[(\mathcal{M}_U^2)_{LR}]_{23}^* [(\mathcal{M}_U^2)_{LR}]_{13}}{M_2^4} l(x_2^Q, x_2^u), \\
 C_3^d &= -\frac{(\alpha_2)^2}{16\sqrt{2}G_F M_W^2} \left(1 - \frac{2}{3} \sin^2 \theta_W\right) \frac{[(\mathcal{M}_U^2)_{LR}]_{23}^* [(\mathcal{M}_U^2)_{LR}]_{13}}{M_2^4} l(x_2^Q, x_2^u), \\
 C_{2,4}^q &= \tilde{C}_{1,2,3,4}^q = 0.
 \end{aligned} \tag{A.2}$$

## A.3 $|\Delta S| = 1$ chromomagnetic dipole contribution

The Wilson coefficients of the chromomagnetic dipole contributions to  $\varepsilon'_K/\varepsilon_K$  are

$$\begin{aligned}
 C_g^- &= \frac{\alpha_s \pi}{3} \frac{\tilde{m}_Q^2 \mu m_s}{M_3^5} (\delta_d^{LL})_{12} \frac{\tan \beta}{1 + \epsilon_g \tan \beta} \left[ I(x_3^Q, x_3^d) + 9J(x_3^Q, x_3^d) \right] \\
 &\quad - \frac{\alpha_s \pi}{3} \frac{\tilde{m}_d^2 \mu m_s}{M_3^5} (\delta_d^{RR})_{12} \frac{\tan \beta}{1 + \epsilon_g \tan \beta} \left[ I(x_3^d, x_3^Q) + 9J(x_3^d, x_3^Q) \right] \\
 &\quad + \frac{\alpha_s \pi}{3} \frac{[(\mathcal{M}_D^2)_{LR}]_{12} - [(\mathcal{M}_D^2)_{LR}]_{21}^*}{M_3^3} \left[ K(x_3^Q, x_3^d) + 9L(x_3^Q, x_3^d) \right] \\
 &\quad - \frac{\alpha_s \pi}{3} \frac{m_s}{\tilde{m}_Q^2} (\delta_d^{LL})_{12} [M_3(x_Q^3) + 9M_4(x_Q^3)] \\
 &\quad + \frac{\alpha_s \pi}{3} \frac{m_s}{\tilde{m}_d^2} (\delta_d^{RR})_{12} [M_3(x_d^3) + 9M_4(x_d^3)].
 \end{aligned} \tag{A.3}$$

## A.4 $|\Delta S| = 2$ gluino box contribution

The Wilson coefficients of the gluino box contributions to  $\varepsilon_K$  are

$$C_1 = -\frac{(\alpha_s)^2}{\tilde{m}_Q^2} [(\delta_d^{LL})_{21}]^2 g_1^{(1)}(x_Q^3), \tag{A.4}$$

$$C_4 = -\frac{(\alpha_s)^2}{M_3^2} [(\delta_d^{LL})_{21} (\delta_d^{RR})_{21}] g_4^{(1)}(x_Q^3, x_d^3), \tag{A.5}$$

$$C_5 \simeq -\frac{(\alpha_s)^2}{M_3^2} [(\delta_d^{LL})_{21} (\delta_d^{RR})_{21}] g_5^{(1)}(x_Q^3, x_d^3), \tag{A.6}$$

$$\tilde{C}_1 = -\frac{(\alpha_s)^2}{\tilde{m}_d^2} [(\delta_d^{RR})_{21}]^2 g_1^{(1)}(x_d^3), \tag{A.7}$$

$$C_2 = C_3 = \tilde{C}_2 = \tilde{C}_3 = 0. \tag{A.8}$$

## A.5 Sub-leading contributions to $\varepsilon_K$

The Wilson coefficients of the Wino and Higgsino contributions are

$$C_1 = -\frac{\alpha_s \alpha_2}{6\tilde{m}_Q^2} [(\delta_d^{LL})_{21}]^2 g_{\tilde{g}\tilde{w}}^{(1)}(x_Q^3, x_Q^2) - \frac{(\alpha_2)^2}{8\tilde{m}_Q^2} [(\delta_d^{LL})_{21}]^2 g_{\tilde{w}}^{(1)}(x_Q^2) - \frac{(\alpha_2)^2}{8\tilde{m}_u^2} (V_{ts}V_{td}^*)^2 \frac{m_t^4}{M_W^4} f_1(x_u^\mu), \quad (\text{A.9})$$

$$\tilde{C}_3 = -\frac{(\alpha_2)^2}{8} (V_{ts}V_{td}^*)^2 \frac{m_s^2 \tan^2 \beta}{(1 + \epsilon_g \tan \beta)^2} \frac{m_t^4}{M_W^4} \frac{\mu^2 A_t^2}{\tilde{m}_Q^4 \tilde{m}_u^4} f_3(x_Q^\mu, x_u^\mu), \quad (\text{A.10})$$

$$C_2 = C_3 = C_4 = C_5 = \tilde{C}_1 = \tilde{C}_2 = 0. \quad (\text{A.11})$$

Note that a  $\tan^4 \beta$  enhanced contribution to  $\varepsilon_K$  comes from the exchange of neutral Higgses, which is discarded because of  $(\delta_d)_{23}(\delta_d)_{31} = 0$  in our analyses. For the Wilson coefficient, we obtain

$$C_2 \simeq \tilde{C}_2 \simeq 0, \quad (\text{A.12})$$

$$C_4 \simeq -\frac{8(\alpha_s)^2 \alpha_2}{9\pi} \frac{m_b^2}{M_W^2} \frac{\tan^4 \beta}{(1 + \epsilon_g \tan \beta)^2 [1 + (\epsilon_g + \epsilon_Y y_t^2) \tan \beta]^2} \frac{\mu^2 M_3^2}{M_A^2 \tilde{m}_Q^2 \tilde{m}_d^2} \times [(\delta_d^{LL})_{23} (\delta_d^{LL})_{31} (\delta_d^{RR})_{23} (\delta_d^{RR})_{31}] H(x_Q^3, x_d^Q) H(x_d^3, x_Q^Q), \quad (\text{A.13})$$

$$C_1 = C_3 = C_5 = \tilde{C}_1 = \tilde{C}_3 = 0, \quad (\text{A.14})$$

where the approximation in eq. (2.41) is used, and the loop function  $H(x, y)$  is given in eq. (B.4). Note that the  $CP$ -even and  $CP$ -odd Higgs contributions to  $C_2$  ( $\tilde{C}_2$ ) are canceled out by each other.

## B Loop functions

### B.1 $K^0 \rightarrow \mu^+ \mu^-$

The loop functions  $l(x, y)$ ,  $F(x, y)$ ,  $G(x, y)$ , and  $H(x, y)$  are given by

$$l(x, y) = -\frac{[x^2 + (x-2)y] x \ln x}{(x-1)^2(x-y)^3} + \frac{[y^2 + (y-2)x] y \ln y}{(y-1)^2(x-y)^3} - \frac{x+y-2xy}{(x-1)(y-1)(x-y)^2}, \quad (\text{B.1})$$

$$F(x, y) = \frac{x \ln x}{(x-1)(x-y)} + \frac{y \ln y}{(y-1)(y-x)}, \quad (\text{B.2})$$

$$G(x, y) = \frac{x \ln x}{(x-1)^2(x-y)} + \frac{y \ln y}{(y-1)^2(y-x)} + \frac{1}{(x-1)(y-1)}, \quad (\text{B.3})$$

$$H(x, y) = \frac{x \ln x}{(x-1)^2(x-y)^2} + \frac{(x+xy-2y^2) \ln y}{(y-1)^3(x-y)^2} - \frac{2x-y-1}{(x-1)(y-1)^2(x-y)}, \quad (\text{B.4})$$

where  $l(1, 1) = -1/12$ ,  $F(1, 1) = 1/2$ ,  $G(1, 1) = -1/6$ , and  $H(1, 1) = 1/12$ .

## B.2 $\varepsilon'_K/\varepsilon_K$

### B.2.1 $|\Delta S| = 1$ gluino box contributions

The loop functions  $f(x, y)$  and  $g(x, y)$  [66] are

$$f(x, y) = \frac{x[2x^2 - (x+1)y] \ln x}{(x-1)^3(x-y)^2} - \frac{xy \ln y}{(y-1)^2(x-y)^2} + \frac{x(x+1-2y)}{(x-1)^2(y-1)(x-y)}, \quad (\text{B.5})$$

$$g(x, y) = -\frac{x^2[x(x+1) - 2y] \ln x}{(x-1)^3(x-y)^2} + \frac{xy^2 \ln y}{(y-1)^2(x-y)^2} + \frac{x[-2x + (x+1)y]}{(x-1)^2(y-1)(x-y)}, \quad (\text{B.6})$$

which lead to

$$f(x, x) = -\frac{1 + 4x - 5x^2 + 2x(2+x) \ln x}{2(x-1)^4} = \frac{1}{x} B_2 \left( \frac{1}{x} \right), \quad (\text{B.7})$$

$$g(x, x) = \frac{x [5 - 4x - x^2 + 2(1+2x) \ln x]}{2(x-1)^4} = -\frac{4}{x} B_1 \left( \frac{1}{x} \right). \quad (\text{B.8})$$

The loop functions  $B_{1,2}(x)$  are consistent with ref. [77] for the universal squark masses case.

### B.2.2 Chromomagnetic-dipole operator

The loop functions  $I(x, y)$ ,  $J(x, y)$ ,  $K(x, y)$ ,  $L(x, y)$ ,  $M_3(x)$ , and  $M_4(x)$  are given by

$$I(x, y) = \frac{(3x^2 - y - 2xy) \ln x}{(x-1)^4(x-y)^2} - \frac{y \ln y}{(y-1)^3(x-y)^2} + \frac{-2 + (-5+x)x + 9y + (2+x)xy - (5+x)y^2}{2(x-y)(x-1)^3(y-1)^2}, \quad (\text{B.9})$$

$$J(x, y) = -\frac{x[(1+2x)x - (2+x)y] \ln x}{(x-1)^4(x-y)^2} + \frac{y^2 \ln y}{(y-1)^3(x-y)^2} + \frac{(5+x)x - 3y(1+x)^2 + (1+5x)y^2}{2(x-1)^3(y-1)^2(x-y)}, \quad (\text{B.10})$$

$$K(x, y) = \frac{x \ln x}{(x-y)(x-1)^3} + \frac{y \ln y}{(y-x)(y-1)^3} + \frac{xy + x + y - 3}{2(x-1)^2(y-1)^2}, \quad (\text{B.11})$$

$$L(x, y) = -\frac{x^2 \ln x}{(x-y)(x-1)^3} - \frac{y^2 \ln y}{(y-x)(y-1)^3} + \frac{1+x+y-3xy}{2(x-1)^2(y-1)^2}, \quad (\text{B.12})$$

$$M_3(x) = \frac{-1 + 9x + 9x^2 - 17x^3 + 6x^2(3+x) \ln x}{12(x-1)^5}, \quad (\text{B.13})$$

$$M_4(x) = \frac{-1 - 9x + 9x^2 + x^3 - 6x(1+x) \ln x}{6(x-1)^5}, \quad (\text{B.14})$$

which lead to

$$K(x, x) = \frac{-5 + 4x + x^2 - 2(1+2x) \ln x}{2(x-1)^4} = \frac{1}{x^2} M_1 \left( \frac{1}{x} \right), \quad (\text{B.15})$$

$$L(x, x) = \frac{1 + 4x - 5x^2 + 2x(2+x) \ln x}{2(x-1)^4} = -\frac{1}{x} B_2 \left( \frac{1}{x} \right). \quad (\text{B.16})$$

The above  $M_{1,3,4}(x)$  are consistent with ref. [77] in the universal squark masses case.<sup>8</sup>

<sup>8</sup>We found that in eq. (14) of ref. [77],  $M_2(x) = -xB_2(x)$  should be replaced by  $M_2(x) = -B_2(x)/x$ , which has been pointed out in ref. [91].

### B.3 $\varepsilon_K$

#### B.3.1 $|\Delta S| = 2$ gluino box contributions

The loop functions  $g_1^{(1)}(x)$ ,  $g_4^{(1)}(x, y)$ , and  $g_5^{(1)}(x, y)$  are given by

$$g_1^{(1)}(x) = -\frac{11 + 144x + 27x^2 - 2x^3}{108(1-x)^4} - \frac{x(13 + 17x)}{18(1-x)^5} \ln x, \quad (\text{B.17})$$

$$\begin{aligned} g_4^{(1)}(x, y) = & -\frac{x^2 y \ln x}{3(x-y)^3(1-x)^3} \{x^2(5+7x) + y[2+7(x-3)x]\} \\ & -\frac{y^2 x \ln y}{3(y-x)^3(1-y)^3} \{y^2(5+7y) + x[2+7(y-3)y]\} \\ & +\frac{xy}{3(1-x)^2(1-y)^2(x-y)^2} (x+y-13x^2-13y^2+8xy+15x^2y+15xy^2-14x^2y^2), \end{aligned} \quad (\text{B.18})$$

$$\begin{aligned} g_5^{(1)}(x, y) = & -\frac{x^2 y \ln x}{9(x-y)^3(1-x)^3} [x^2(11+x) + (x-5)(x+2)y] \\ & -\frac{y^2 x \ln y}{9(y-x)^3(1-y)^3} [y^2(11+y) + (y-5)(y+2)x] \\ & -\frac{xy}{9(1-x)^2(1-y)^2(x-y)^2} (5x+5y+7x^2+7y^2-32xy+3x^2y+3xy^2+2x^2y^2). \end{aligned} \quad (\text{B.19})$$

#### B.3.2 Wino and Higgsino contributions

The loop functions  $g_{\tilde{g}\tilde{w}}^{(1)}$ ,  $g_{\tilde{w}}^{(1)}(x)$ ,  $f_1(x)$  and  $f_3(x, y)$  are given by

$$\begin{aligned} g_{\tilde{g}\tilde{w}}^{(1)}(x, y) = & -\sqrt{xy} \left[ \frac{x \ln x}{(x-y)(1-x)^4} + \frac{y \ln y}{(y-x)(1-y)^4} \right. \\ & \left. + \frac{11 - 7(x+y) + 2(x^2 + y^2) - 10xy + 5xy(x+y) - x^2y^2}{6(1-x)^3(1-y)^3} \right] \\ & -\frac{x^2 \ln x}{2(x-y)(1-x)^4} - \frac{y^2 \ln y}{2(y-x)(1-y)^4} \\ & -\frac{2 + 5(x+y) - (x^2 + y^2) - 22xy + 5xy(x+y) + 2x^2y^2}{12(1-x)^3(1-y)^3}, \end{aligned} \quad (\text{B.20})$$

$$g_{\tilde{w}}^{(1)}(x) = \frac{-5 - 67x - 13x^2 + x^3}{12(1-x)^4} - \frac{x(3 + 4x)}{(1-x)^5} \ln x, \quad (\text{B.21})$$

$$f_1(x) = -\frac{x+1}{4(1-x)^2} - \frac{x}{2(1-x)^3} \ln x, \quad (\text{B.22})$$

$$\begin{aligned} f_3(x, y) = & -\frac{x^2[x(1+x+y) - 3y]}{(x-y)^3(1-x)^3} \ln x - \frac{y^2[y(1+x+y) - 3x]}{(y-x)^3(1-y)^3} \ln y \\ & -2\frac{x^2 + y^2 - xy - x^2y - xy^2 + x^2y^2}{(1-x)^2(1-y)^2(x-y)^2}, \end{aligned} \quad (\text{B.23})$$

$$f_3(x) = \frac{x^2 - 8x - 17}{6(1-x)^4} - \frac{3x + 1}{(1-x)^5} \ln x, \quad (\text{B.24})$$

where  $\lim_{y \rightarrow x} f_3(x, y) = f_3(x)$ .<sup>9</sup>

<sup>9</sup>We found that in eq. (A.15) in ref. [25],  $f_3(x) = (x^2 - 6x - 17)/[6(1-x)^4] - (3x + 1) \ln x / (1-x)^5$  should be replaced by eq. (B.24).

**Open Access.** This article is distributed under the terms of the Creative Commons Attribution License ([CC-BY 4.0](https://creativecommons.org/licenses/by/4.0/)), which permits any use, distribution and reproduction in any medium, provided the original author(s) and source are credited.

## References

- [1] C. Hamzaoui, M. Pospelov and M. Toharia, *Higgs mediated FCNC in supersymmetric models with large tan Beta*, *Phys. Rev. D* **59** (1999) 095005 [[hep-ph/9807350](#)] [[INSPIRE](#)].
- [2] K.S. Babu and C.F. Kolda, *Higgs mediated  $B^0 \rightarrow \mu^+\mu^-$  in minimal supersymmetry*, *Phys. Rev. Lett.* **84** (2000) 228 [[hep-ph/9909476](#)] [[INSPIRE](#)].
- [3] P.H. Chankowski and L. Slawianowska,  *$B_{d,s}^0 \rightarrow \mu^-\mu^+$  decay in the MSSM*, *Phys. Rev. D* **63** (2001) 054012 [[hep-ph/0008046](#)] [[INSPIRE](#)].
- [4] C. Bobeth, T. Ewerth, F. Krüger and J. Urban, *Analysis of neutral Higgs boson contributions to the decays  $\bar{B}(s) \rightarrow \ell^+\ell^-$  and  $\bar{B} \rightarrow K\ell^+\ell^-$* , *Phys. Rev. D* **64** (2001) 074014 [[hep-ph/0104284](#)] [[INSPIRE](#)].
- [5] G. Isidori and A. Retico, *Scalar flavor changing neutral currents in the large tan  $\beta$  limit*, *JHEP* **11** (2001) 001 [[hep-ph/01110121](#)] [[INSPIRE](#)].
- [6] G. Isidori and A. Retico,  *$B_{s,d} \rightarrow \ell^+\ell^-$  and  $K_L \rightarrow \ell^+\ell^-$  in SUSY models with nonminimal sources of flavor mixing*, *JHEP* **09** (2002) 063 [[hep-ph/0208159](#)] [[INSPIRE](#)].
- [7] A. Crivellin, *Effective Higgs vertices in the generic MSSM*, *Phys. Rev. D* **83** (2011) 056001 [[arXiv:1012.4840](#)] [[INSPIRE](#)].
- [8] A. Crivellin, L. Hofer and J. Rosiek, *Complete resummation of chirally-enhanced loop-effects in the MSSM with non-minimal sources of flavor-violation*, *JHEP* **07** (2011) 017 [[arXiv:1103.4272](#)] [[INSPIRE](#)].
- [9] A. Crivellin and C. Greub, *Two-loop supersymmetric QCD corrections to Higgs-quark-quark couplings in the generic MSSM*, *Phys. Rev. D* **87** (2013) 015013 [*Erratum ibid.* **D 87** (2013) 079901] [[arXiv:1210.7453](#)] [[INSPIRE](#)].
- [10] S.R. Choudhury and N. Gaur, *Dileptonic decay of  $B_s$  meson in SUSY models with large tan  $\beta$* , *Phys. Lett. B* **451** (1999) 86 [[hep-ph/9810307](#)] [[INSPIRE](#)].
- [11] C.-S. Huang, W. Liao, Q.-S. Yan and S.-H. Zhu,  *$B_s \rightarrow \ell^+\ell^-$  in a general 2 HDM and MSSM*, *Phys. Rev. D* **63** (2001) 114021 [*Erratum ibid.* **D 64** (2001) 059902] [[hep-ph/0006250](#)] [[INSPIRE](#)].
- [12] Z. Xiong and J.M. Yang,  *$B$  meson dileptonic decays enhanced by supersymmetry with large tan  $\beta$* , *Nucl. Phys. B* **628** (2002) 193 [[hep-ph/0105260](#)] [[INSPIRE](#)].
- [13] A. Dedes, H.K. Dreiner and U. Nierste, *Correlation of  $B_s \rightarrow \mu^+\mu^-$  and  $(g-2)_\mu$  in minimal supergravity*, *Phys. Rev. Lett.* **87** (2001) 251804 [[hep-ph/0108037](#)] [[INSPIRE](#)].
- [14] C. Bobeth, T. Ewerth, F. Krüger and J. Urban, *Enhancement of  $B(\bar{B}_d \rightarrow \mu^+\mu^-)/B(\bar{B}_s \rightarrow \mu^+\mu^-)$  in the MSSM with minimal flavor violation and large tan beta*, *Phys. Rev. D* **66** (2002) 074021 [[hep-ph/0204225](#)] [[INSPIRE](#)].
- [15] S. Baek, P. Ko and W.Y. Song, *Implications on SUSY breaking mediation mechanisms from observing  $B_s \rightarrow \mu^+\mu^-$  and the muon  $(g-2)$* , *Phys. Rev. Lett.* **89** (2002) 271801 [[hep-ph/0205259](#)] [[INSPIRE](#)].
- [16] A. Dedes, H.K. Dreiner, U. Nierste and P. Richardson, *Trilepton events and  $B_s \rightarrow \mu^+\mu^-$ : no lose for mSUGRA at the Tevatron?*, [hep-ph/0207026](#) [[INSPIRE](#)].

- [17] J.K. Mizukoshi, X. Tata and Y. Wang, *Higgs mediated leptonic decays of  $B_s$  and  $B_d$  mesons as probes of supersymmetry*, *Phys. Rev. D* **66** (2002) 115003 [[hep-ph/0208078](#)] [[INSPIRE](#)].
- [18] S. Baek, P. Ko and W.Y. Song, *SUSY breaking mediation mechanisms and  $(g-2)_\mu$ ,  $B \rightarrow X_s \gamma$ ,  $B \rightarrow X_s \ell^+ \ell^-$  and  $B_s \rightarrow \mu^+ \mu^-$* , *JHEP* **03** (2003) 054 [[hep-ph/0208112](#)] [[INSPIRE](#)].
- [19] G. Ecker and A. Pich, *The Longitudinal muon polarization in  $K_L \rightarrow \mu^+ \mu^-$* , *Nucl. Phys. B* **366** (1991) 189 [[INSPIRE](#)].
- [20] G. Isidori and R. Unterdorfer, *On the short distance constraints from  $K_{L,S} \rightarrow \mu^+ \mu^-$* , *JHEP* **01** (2004) 009 [[hep-ph/0311084](#)] [[INSPIRE](#)].
- [21] G. D'Ambrosio and T. Kitahara, *Direct CP violation in  $K \rightarrow \mu^+ \mu^-$* , *Phys. Rev. Lett.* **119** (2017) 201802 [[arXiv:1707.06999](#)] [[INSPIRE](#)].
- [22] R. Aaij et al., *Improved limit on the branching fraction of the rare decay  $K_S^0 \rightarrow \mu^+ \mu^-$* , *Eur. Phys. J. C* **77** (2017) 678.
- [23] D. Martinez-Santos, *Physics of LHCb upgrade(s)*, [LHCb-TALK-2017-164](#) (2017).
- [24] L. Hall, V. Kostelecky, and S. Raby, *New flavor violations in supergravity models*, *Nucl. Phys. B* **267** (1986) 415.
- [25] W. Altmannshofer et al., *Anatomy and phenomenology of FCNC and CPV effects in SUSY theories*, *Nucl. Phys. B* **830** (2010) 17 [[arXiv:0909.1333](#)] [[INSPIRE](#)].
- [26] J. Rosiek, *Complete set of Feynman rules for the MSSM: erratum*, [hep-ph/9511250](#) [[INSPIRE](#)].
- [27] B.C. Allanach et al., *SUSY Les Houches accord 2*, *Comput. Phys. Commun.* **180** (2009) 8 [[arXiv:0801.0045](#)] [[INSPIRE](#)].
- [28] A. Crivellin, G. D'Ambrosio, T. Kitahara and U. Nierste,  *$K \rightarrow \pi \nu \bar{\nu}$  in the MSSM in light of the  $\epsilon'_K/\epsilon_K$  anomaly*, *Phys. Rev. D* **96** (2017) 015023 [[arXiv:1703.05786](#)] [[INSPIRE](#)].
- [29] T. Blum et al., *The  $K \rightarrow (\pi\pi)_{I=2}$  decay amplitude from lattice QCD*, *Phys. Rev. Lett.* **108** (2012) 141601 [[arXiv:1111.1699](#)] [[INSPIRE](#)].
- [30] T. Blum et al., *Lattice determination of the  $K \rightarrow (\pi\pi)_{I=2}$  decay amplitude  $A_2$* , *Phys. Rev. D* **86** (2012) 074513 [[arXiv:1206.5142](#)] [[INSPIRE](#)].
- [31] T. Blum et al.,  *$K \rightarrow \pi\pi$   $\Delta I = 3/2$  decay amplitude in the continuum limit*, *Phys. Rev. D* **91** (2015) 074502 [[arXiv:1502.00263](#)] [[INSPIRE](#)].
- [32] RBC, UKQCD collaboration, Z. Bai et al., *Standard model prediction for direct CP-violation in  $K \rightarrow \pi\pi$  decay*, *Phys. Rev. Lett.* **115** (2015) 212001 [[arXiv:1505.07863](#)] [[INSPIRE](#)].
- [33] E. Pallante, A. Pich and I. Scimemi, *The standard model prediction for  $\epsilon'/\epsilon$* , *Nucl. Phys. B* **617** (2001) 441 [[hep-ph/0105011](#)] [[INSPIRE](#)].
- [34] T. Hambye, S. Peris and E. de Rafael,  *$\Delta I = 1/2$  and  $\epsilon'/\epsilon$  in large  $N_c$  QCD*, *JHEP* **05** (2003) 027 [[hep-ph/0305104](#)] [[INSPIRE](#)].
- [35] H.G. Mullor, *Updated standard model prediction for the kaon direct CP-violating ratio  $\epsilon'_k/\epsilon_k$* , talk given at the *IX CPAN DAYS*, October 23–25, Santander, Spain (2017).
- [36] G. D'Ambrosio, G. Ecker, G. Isidori and H. Neufeld, *Radiative nonleptonic kaon decays*, [hep-ph/9411439](#) [[INSPIRE](#)].
- [37] PARTICLE DATA GROUP Collaboration, C. Patrignani et al., *Review of particle physics*, *Chin. Phys. C* **40** (2016) 100001.
- [38] SWME collaboration, Y.-C. Jang et al., *Update on  $\epsilon_K$  with lattice QCD inputs*, *EPJ Web Conf.* **175** (2018) 14015 [[arXiv:1710.06614](#)] [[INSPIRE](#)].

- [39] M. Endo et al., *Glino-mediated electroweak penguin with flavor-violating trilinear couplings*, *JHEP* **04** (2018) 019 [[arXiv:1712.04959](#)].
- [40] T. Kitahara, U. Nierste and P. Tremper, *Singularity-free next-to-leading order  $\Delta S = 1$  renormalization group evolution and  $\epsilon'_K/\epsilon_K$  in the Standard Model and beyond*, *JHEP* **12** (2016) 078 [[arXiv:1607.06727](#)] [[INSPIRE](#)].
- [41] S. Descotes-Genon, L. Hofer, J. Matias and J. Virto, *Global analysis of  $b \rightarrow s\ell\ell$  anomalies*, *JHEP* **06** (2016) 092 [[arXiv:1510.04239](#)] [[INSPIRE](#)].
- [42] ATLAS collaboration, *Search for additional heavy neutral Higgs and gauge bosons in the ditau final state produced in  $36\text{fb}^{-1}$  of  $pp$  collisions at  $\sqrt{s} = 13$  TeV with the ATLAS detector*, *JHEP* **01** (2018) 055 [[arXiv:1709.07242](#)] [[INSPIRE](#)].
- [43] A.J. Buras et al., *Connections between  $\epsilon'/\epsilon$  and rare kaon decays in supersymmetry*, *Nucl. Phys. B* **566** (2000) 3 [[hep-ph/9908371](#)] [[INSPIRE](#)].
- [44] R. Barbieri, R. Contino and A. Strumia,  *$\epsilon'$  from supersymmetry with nonuniversal  $A$  terms?*, *Nucl. Phys. B* **578** (2000) 153 [[hep-ph/9908255](#)] [[INSPIRE](#)].
- [45] F. Mescia, C. Smith and S. Trine,  *$K_L \rightarrow \pi^0 e^+ e^-$  and  $K_L \rightarrow \pi^0 \mu^+ \mu^-$ : a binary star on the stage of flavor physics*, *JHEP* **08** (2006) 088 [[hep-ph/0606081](#)] [[INSPIRE](#)].
- [46] W. Altmannshofer, P. Paradisi and D.M. Straub, *Model-Independent constraints on new physics in  $b \rightarrow s$  transitions*, *JHEP* **04** (2012) 008 [[arXiv:1111.1257](#)] [[INSPIRE](#)].
- [47] A.J. Buras, R. Fleischer, J. Girrbach and R. Knegjens, *Probing new physics with the  $B_s \rightarrow \mu^+ \mu^-$  time-dependent rate*, *JHEP* **07** (2013) 77 [[arXiv:1303.3820](#)] [[INSPIRE](#)].
- [48] A. Crivellin, J. Heeck and D. Müller, *Large  $h \rightarrow bs$  in generic two-Higgs-doublet models*, *Phys. Rev. D* **97** (2018) 035008 [[arXiv:1710.04663](#)] [[INSPIRE](#)].
- [49] G. Isidori, C. Smith and R. Unterdorfer, *The rare decay  $K_L \rightarrow \pi^0 \mu^+ \mu^-$  within the SM*, *Eur. Phys. J. C* **36** (2004) 57 [[hep-ph/0404127](#)] [[INSPIRE](#)].
- [50] D. Gomez Dumm and A. Pich, *Long distance contributions to the  $K_L \rightarrow \mu^+ \mu^-$  decay width*, *Phys. Rev. Lett.* **80** (1998) 4633 [[hep-ph/9801298](#)] [[INSPIRE](#)].
- [51] M. Knecht, S. Peris, M. Perrottet and E. de Rafael, *Decay of pseudoscalars into lepton pairs and large  $N_c$  QCD*, *Phys. Rev. Lett.* **83** (1999) 5230 [[hep-ph/9908283](#)] [[INSPIRE](#)].
- [52] A. Pich and E. de Rafael, *Weak  $K$  amplitudes in the chiral and  $1/N_c$  expansions*, *Phys. Lett. B* **374** (1996) 186 [[hep-ph/9511465](#)] [[INSPIRE](#)].
- [53] J.-M. Gerard, C. Smith and S. Trine, *Radiative kaon decays and the penguin contribution to the  $\Delta I = 1/2$  rule*, *Nucl. Phys. B* **730** (2005) 1 [[hep-ph/0508189](#)] [[INSPIRE](#)].
- [54] M. Gorbahn and U. Haisch, *Charm quark contribution to  $K_L \rightarrow \mu^+ \mu^-$  at next-to-next-to-leading*, *Phys. Rev. Lett.* **97** (2006) 122002 [[hep-ph/0605203](#)] [[INSPIRE](#)].
- [55] G. Colangelo, R. Stucki and L.C. Tunstall, *Dispersive treatment of  $K_S \rightarrow \gamma\gamma$  and  $K_S \rightarrow \gamma\ell^+\ell^-$* , *Eur. Phys. J. C* **76** (2016) 604 [[arXiv:1609.03574](#)] [[INSPIRE](#)].
- [56] G. Colangelo and G. Isidori, *Supersymmetric contributions to rare kaon decays: Beyond the single mass insertion approximation*, *JHEP* **09** (1998) 009 [[hep-ph/9808487](#)] [[INSPIRE](#)].
- [57] M. Endo, S. Mishima, D. Ueda and K. Yamamoto, *Chargino contributions in light of recent  $\epsilon'/\epsilon$* , *Phys. Lett. B* **762** (2016) 493 [[arXiv:1608.01444](#)] [[INSPIRE](#)].
- [58] A.J. Buras, M. Gorbahn, S. Jäger and M. Jamin, *Improved anatomy of  $\epsilon'_K/\epsilon_K$  in the standard model*, *JHEP* **11** (2015) 202 [[arXiv:1507.06345](#)] [[INSPIRE](#)].
- [59] A.J. Buras and J.-M. Gerard, *Upper bounds on  $\epsilon'_K/\epsilon_K$  parameters  $B_6^{(1/2)}$  and  $B_8^{(3/2)}$  from large  $N$  QCD and other news*, *JHEP* **12** (2015) 008 [[arXiv:1507.06326](#)] [[INSPIRE](#)].



- [60] A.J. Buras and J.-M. Gerard, *Final state interactions in  $K \rightarrow \pi\pi$  decays:  $\Delta I = 1/2$  rule vs.  $\epsilon'/\epsilon$* , *Eur. Phys. J. C* **77** (2017) 10 [[arXiv:1603.05686](#)] [[INSPIRE](#)].
- [61] L. Lellouch and M. Lüscher, *Weak transition matrix elements from finite volume correlation functions*, *Commun. Math. Phys.* **219** (2001) 31 [[hep-lat/0003023](#)] [[INSPIRE](#)].
- [62] G. Colangelo, J. Gasser and H. Leutwyler,  *$\pi\pi$  scattering*, *Nucl. Phys. B* **603** (2001) 125 [[hep-ph/0103088](#)] [[INSPIRE](#)].
- [63] R. Garcia-Martin et al., *The Pion-pion scattering amplitude. IV: improved analysis with once subtracted Roy-like equations up to 1100 MeV*, *Phys. Rev. D* **83** (2011) 074004 [[arXiv:1102.2183](#)] [[INSPIRE](#)].
- [64] G. Colangelo,  *$\pi$ - $\pi$  phase from hadronic &  $K14$  decays*, talk given at the *NA62 Physics Handbook MITP Workshop*, December 10–12, CERN, Switzerland (2016).
- [65] T. Kitahara, U. Nierste and P. Tremper, *Supersymmetric explanation of CP-violation in  $K \rightarrow \pi\pi$  decays*, *Phys. Rev. Lett.* **117** (2016) 091802 [[arXiv:1604.07400](#)] [[INSPIRE](#)].
- [66] A.L. Kagan and M. Neubert, *Large  $\Delta I = 3/2$  contribution to  $\epsilon'_K/\epsilon$  in supersymmetry*, *Phys. Rev. Lett.* **83** (1999) 4929 [[hep-ph/9908404](#)] [[INSPIRE](#)].
- [67] V. Cirigliano, A. Pich, G. Ecker and H. Neufeld, *Isospin violation in  $\epsilon'_K$* , *Phys. Rev. Lett.* **91** (2003) 162001 [[hep-ph/0307030](#)] [[INSPIRE](#)].
- [68] V. Cirigliano, G. Ecker, H. Neufeld and A. Pich, *Isospin breaking in  $K \rightarrow \pi\pi$  decays*, *Eur. Phys. J. C* **33** (2004) 369 [[hep-ph/0310351](#)] [[INSPIRE](#)].
- [69] SWME collaboration, J.A. Bailey et al., *Standard Model evaluation of  $\epsilon_K$  using lattice QCD inputs for  $\hat{B}_K$  and  $V_{cb}$* , *Phys. Rev. D* **92** (2015) 034510 [[arXiv:1503.05388](#)] [[INSPIRE](#)].
- [70] HFLAV collaboration, Y. Amhis et al., *Averages of b-hadron, c-hadron and  $\tau$ -lepton properties as of summer 2016*, *Eur. Phys. J. C* **77** (2017) 895 [[arXiv:1612.07233](#)] [[INSPIRE](#)].
- [71] D. Bigi, P. Gambino and S. Schacht, *A fresh look at the determination of  $|V_{cb}|$  from  $B \rightarrow D^* \ell \nu$* , *Phys. Lett. B* **769** (2017) 441 [[arXiv:1703.06124](#)] [[INSPIRE](#)].
- [72] B. Grinstein and A. Kobach, *Model-independent extraction of  $|V_{cb}|$  from  $\bar{B} \rightarrow D^* \ell \bar{\nu}$* , *Phys. Lett. B* **771** (2017) 359 [[arXiv:1703.08170](#)] [[INSPIRE](#)].
- [73] F.U. Bernlochner, Z. Ligeti, M. Papucci and D.J. Robinson, *Tensions and correlations in  $|V_{cb}|$  determinations*, *Phys. Rev. D* **96** (2017) 091503 [[arXiv:1708.07134](#)] [[INSPIRE](#)].
- [74] A. Bevan et al., *Standard Model updates and new physics analysis with the unitarity triangle fit*, *Nucl. Phys. Proc. Suppl.* **241-242** (2013) 89 [[INSPIRE](#)].
- [75] KLOE collaboration, F. Ambrosino et al., *Determination of CP and CPT violation parameters in the neutral kaon system using the Bell-Steinberger relation and data from the KLOE experiment*, *JHEP* **12** (2006) 011 [[hep-ex/0610034](#)] [[INSPIRE](#)].
- [76] A. Crivellin and M. Davidkov, *Do squarks have to be degenerate? Constraining the mass splitting with Kaon and D mixing*, *Phys. Rev. D* **81** (2010) 095004 [[arXiv:1002.2653](#)] [[INSPIRE](#)].
- [77] F. Gabbiani, E. Gabrielli, A. Masiero and L. Silvestrini, *A complete analysis of FCNC and CP constraints in general SUSY extensions of the standard model*, *Nucl. Phys. B* **477** (1996) 321 [[hep-ph/9604387](#)] [[INSPIRE](#)].
- [78] A.J. Buras, D. Guadagnoli and G. Isidori, *On  $\epsilon_K$  beyond lowest order in the operator product expansion*, *Phys. Lett. B* **688** (2010) 309 [[arXiv:1002.3612](#)] [[INSPIRE](#)].

- [79] RBC/UKQCD collaboration, N. Garron, R.J. Hudspith and A.T. Lytle, *Neutral kaon mixing beyond the standard model with  $N_f = 2 + 1$  chiral fermions part 1: bare matrix elements and physical results*, *JHEP* **11** (2016) 001 [[arXiv:1609.03334](#)] [[INSPIRE](#)].
- [80] J.A. Bagger, K.T. Matchev and R.-J. Zhang, *QCD corrections to flavor changing neutral currents in the supersymmetric standard model*, *Phys. Lett. B* **412** (1997) 77 [[hep-ph/9707225](#)] [[INSPIRE](#)].
- [81] D.M. Santos et al., *Ipanema- $\beta$ : tools and examples for HEP analysis on GPU*, [arXiv:1706.01420](#) [[INSPIRE](#)].
- [82] J. Brest et al., *Self-adapting control parameters in differential evolution: a comparative study on numerical benchmark problems*, *IEEE Trans. Evol. Comput.* **10** (2006) 646.
- [83] P.A.R. Ade et al., *Planck 2015 results xiii. cosmological parameters*, *Astron. Astrophys.* **594** (2016) A13.
- [84] J.C. Costa et al., *Likelihood analysis of the sub-GUT MSSM in light of LHC 13 TeV data*, *Eur. Phys. J. C* **78** (2018) 158 [[arXiv:1711.00458](#)] [[INSPIRE](#)].
- [85] E. Bagnaschi et al., *Likelihood analysis of the pMSSM11 in light of LHC 13 TeV data*, *Eur. Phys. J. C* **78** (2018) 256 [[arXiv:1710.11091](#)] [[INSPIRE](#)].
- [86] E.A. Bagnaschi et al., *Supersymmetric dark matter after LHC Run 1*, *Eur. Phys. J. C* **75** (2015) 500 [[arXiv:1508.01173](#)] [[INSPIRE](#)].
- [87] E. Bagnaschi et al., *Likelihood analysis of the minimal AMSB model*, *Eur. Phys. J. C* **77** (2017) 268 [[arXiv:1612.05210](#)] [[INSPIRE](#)].
- [88] A. Cuoco, J. Heisig, M. Korsmeier and M. Krämer, *Constraining heavy dark matter with cosmic-ray antiprotons*, *JCAP* **04** (2018) 004 [[arXiv:1711.05274](#)] [[INSPIRE](#)].
- [89] J. Hisano, S. Matsumoto, M. Nagai, O. Saito and M. Senami, *Non-perturbative effect on thermal relic abundance of dark matter*, *Phys. Lett. B* **646** (2007) 34 [[hep-ph/0610249](#)] [[INSPIRE](#)].
- [90] M. Ibe, S. Matsumoto and R. Sato, *Mass splitting between charged and neutral Winos at two-loop level*, *Phys. Lett. B* **721** (2013) 252 [[arXiv:1212.5989](#)] [[INSPIRE](#)].
- [91] R. Harnik, D.T. Larson, H. Murayama and A. Pierce, *Atmospheric neutrinos can make beauty strange*, *Phys. Rev. D* **69** (2004) 094024 [[hep-ph/0212180](#)] [[INSPIRE](#)].